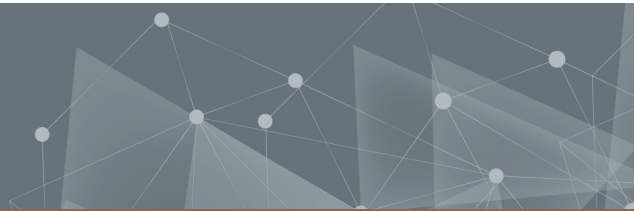




CHALMERS
UNIVERSITY OF TECHNOLOGY



placeholder figure

Nucleation of lithium ...

Understanding of nucleation in future lithium-metal batteries

Master's thesis in Physics

GOTTFRID OLSSON

DEPARTMENT OF PHYSICS

CHALMERS UNIVERSITY OF TECHNOLOGY
Gothenburg, Sweden 2024
www.chalmers.se

MASTER'S THESIS 2024

Nucleation of lithium ...

Understanding of nucleation in future lithium-metal batteries

GOTTFRID OLSSON



Department of Physics
Division of Materials Physics
CHALMERS UNIVERSITY OF TECHNOLOGY
Gothenburg, Sweden 2024

Nucleation of lithium ...
Understanding of nucleation in future lithium-metal batteries
GOTTFRID OLSSON

© GOTTFRID OLSSON, 2024.

Supervisor: Josef Rizell, Department of Physics
Examiner: Alexander Matic, Department of Physics

Master's Thesis 2024
Department of Physics
Division of Materials Physics
Chalmers University of Technology
SE-412 96 Gothenburg

Cover: ***explain front cover***.
Cover figure created by Gottfrid Olsson.

Typeset in L^AT_EX
Printed by Chalmers digitaltryck.
Gothenburg, Sweden 2024

Nucleation of lithium ...
Understanding of nucleation in future lithium-metal batteries
GOTTFRID OLSSON
Department of Physics

Abstract

- * why batteries? * why LMBs? * why nucleation important?
- * what was done, researched?
- * conclusions drawn?

Keywords: lithium-metal battery, nucleation, scanning electron microscopy, deposition, lithium, copper, ...

Acknowledgements

My gratitude goes out to my supervisor Josef Rizell, who not only taught me the essentials of battery research in the lab, but was also always available for discussion and brightened each day with an encouraging and positive attitude. Moreover, I am thankful for the support of my examiner Aleksandar Matic, who helped guide this project with ideas and encouragement. I have to mention the lovely people of the material physics department – it has been wonderful to get to know and work with you. Lastly, I offer my thanks to the friends who have given constructive feedback on my figures, making them ever more pedagogical and elegant.

Gottfrid Olsson, Gothenburg, May 2024

Contents

Contents

1	Introduction	1
2	Lithium batteries	3
2.1	History of batteries and use today	3
2.2	Battery concepts with a lithium-ion battery (LIB) example	4
2.3	Lithium-metal battery (LMB) example	9
2.3.1	Problems with non-uniform lithium deposition	10
3	Nucleation	13
3.1	Steps during nucleation and growth	13
3.2	Deposition curve in a cell	14
3.3	Homogenous nucleation theory	16
3.4	Specific scientific questions in this work	18
4	Methods	21
4.1	Material preparation	22
4.1.1	Electrode materials	22
4.1.2	Electrolytes	22
4.2	Cell configurations and assembly	24
4.2.1	The coin cell (C-cell)	24
4.2.2	The Swagelok two-electrode cell (I-cell)	26
4.2.3	The Swagelok three-electrode cell (T-cell)	28
4.3	Electrochemical cycling of the cells	30
4.3.1	Cycling protocol for SEM images	30
4.3.2	Cycling protocol for electrochemical measurements	31
4.3.3	Sample preparation for SEM	31
4.4	Electron microscopy	32
4.4.1	Scanning electron microscope (SEM)	32
4.5	Data analysis	35

4.5.1	Quantities from/treatment of SEM images	35
4.5.2	Treatment of electrochemical data	35
5	Results and discussion	37
5.1	SEM images	37
5.2	Electrochemical plots	46
5.2.1	Deposition for different degrees of substrate passivation . . .	46
5.2.2	Current density and cell configuration	48
5.2.3	Different electrolytes	53
6	Conclusions	55
References		57
A	Supplementary information: methods	I
A.1	Polishing of Cu	II
A.2	Polypropylene spacer for T-cell	IV

Introduction

Batteries play an important role in our society, being used in things from mobile phones, hearing aids and pacemakers [1], to power tools [2], emergency power [2], electric vehicles [3], and even in space exploration [4], [5]. A battery is a device consisting of several cells, where each cell stores chemical energy that can be extracted as electricity [6]. lithium-ion batteries (LIBs) are one of the most widely used types of batteries, with billions of cells being produced each year [7]. The popularity stems from LIBs favorable properties, in particular its high energy density, high efficiency, and long cycle life [7]. However, the need for even better lithium-based batteries are growing due to increasing demands [3]. Electrical vehicles, for example, would gain the benefit of increased range from batteries with higher energy densities and higher specific energies [8].

One example of a battery utilizing the high specific capacity (mAh g^{-1}) of lithium (Li) is a lithium-metal battery (LMB). A LMB is, simply put, a LIB where the graphite (372 mAh g^{-1} for LiC_6) has been replaced with Li-metal (3862 mAh g^{-1}). This replacement can double the energy density from 600 Wh L^{-1} to 1200 Wh L^{-1} [2] and increase the specific energy of the cell from 250 Wh kg^{-1} to 440 Wh kg^{-1} [9]. However, there is a problem. In a LIB, the Li is inserted between the graphite layers, whereas the Li gets deposited directly on the electrode surface in a LMB. When this Li-metal grows, it can grow unevenly, resulting in a non-uniform deposition. This non-uniform deposition leads to low Coulombic efficiency due to "dead" Li [10]–[13], a short cycle life [10], [11], and is a safety risk by enabling Li-growth that can short-circuit the cell [10]–[12]. This uneven deposition of Li is considered a large obstacle for practical application of Li-metal in batteries [13]–[15].

In order to solve this problem of uneven deposition, the process must first be well understood. Studies have been conducted on both the nucleation and growth of Li-metal [16]–[19]. The first step, nucleation of Li, is important since the initial nuclei influences the growth and subsequent resulting morphology of the deposition as a whole. More knowledge about the process can therefore lead to ways of enabling more even and regular nucleation and growth in LMBs, which would improve their performance. This work focuses on investigating the nucleation behavior.

The purpose of this work is to investigate how the nucleation in Li-metal cells can be affected. Specifically, electron microscopy will be used to image Li nuclei in different cell configurations, and electrochemical cycling will be performed to investigate the nucleation behavior in different cell configurations as function of current density with different levels of passivation of the counter electrode surface.

2

Lithium batteries

In this section, a short history of batteries and their use today is first given. Thereafter, fundamental battery concepts are explained, with an example of the LIB since it is both instructive and a common battery type. Relevant theoretical ideas are then introduced, such as the cell potential, Gibbs free energy, and overpotential, of which the last two will be central for understanding nucleation. Finally, a LMB example showcases problems associated with non-uniform deposition of Li.

2.1 History of batteries and use today

The history of batteries always starts with Alessandro Volta, who in 1800 created an "electric pile" in order to settle an intellectual dispute [1]. The pile was the world's first battery¹ and consisted of alternating disks of silver and zinc, with cloths soaked in salt water in between [1]. Volta's pile demonstrated that electrical energy could be stored in and extracted from metals and electrolytes (liquids with ions). Several different rechargeable batteries were invented thereafter, for instance the lead-acid battery (1859) [1], the nickel-cadmium battery (1901) [1], and the lithium-ion battery (1991²) [2]. These earlier types of batteries have been

¹The word "battery" for such a device was coined by Benjamin Franklin (as a play on the military term) in 1748 when describing his experiments with an "electrical battery" [20]. Franklin's electrical battery consisted of eleven large glass panes, with lead on each side, placed close to each other in series (a series of capacitors) [20]. Others had experimented with electrical batteries before, most notably Johann Heinrich Winkler and Daniel Gralath, both in 1746 [20].

²The earliest functioning rechargeable lithium battery came during the 1970s. However, what we today call a rechargeable LIB was first patented in 1991 [21], by then standing on the shoulders of decades worth of lithium battery research [2], [21].

improved on during the years and are still in use today. For example, lead-acid batteries ignites car engines and drives industrial trucks [2], while nickel-cadmium batteries are used in power tools and as emergency power [2]. LIBs can be found everywhere, some examples already mentioned are in consumer electronics such as mobile phones, watches, and laptops, but is also used in power tools, electrical vehicles [1], and space exploration [4].

2.2 Battery concepts with a lithium-ion battery (LIB) example

Li is considered one of the top candidates for high-energy batteries is due to its favorable properties. To understand this, the quantity capacity is introduced. Capacity is a material's ability to store charge and is measured in milliampere hours (1 mAh is equal to 3.6 C, or 10^{19} electrons³). A material's specific capacity is its capacity divided by its mass (mAh g^{-1}), and a high specific capacity means more energy stored per mass of material. Compared to all other elements, for example sodium (1166 mAh g^{-1}), potassium (685 mAh g^{-1}), nickel (457 mAh g^{-1}), cadmium (238 mAh g^{-1}) and lead (129 mAh g^{-1}), Li has the highest theoretical capacity⁴ of 3860 mAh g^{-1} . Li is a compelling candidate for high-energy batteries for this reason, and also for its other favorable properties like low standard electrode potential (−3.04 V against the standard hydrogen electrode) [9] and low density (0.534 g cm^{-3} , almost half that of water) [10]. The high theoretical capacity increases the specific energy (Wh kg^{-1}) of the cell, while the low density of Li increases the energy density (Wh L^{-1}) of the cell. Low standard electrode potential help increases both these quantities.

As mentioned, a battery is a device that consists of several cells, where each cell stores chemical energy that can be extracted as electricity [6]. A cell, in turn, is made up of several parts, as illustrated in Figure 2.1. The electrode materials, here graphite and LiCoO_2 (LCO), are electrically conductive and provides the materials necessary for electrochemical reactions to occur. Between the electrodes is an electrolyte and a separator. The separator keeps the electrodes from touching each other and thereby short-circuiting, while the electrolyte prevents electrons (e^-) from passing through, but allows ions (such as Li^+), to move between the electrodes. The last components are the current collectors, here copper (Cu) and

³This is a huge number. If you had 10^{19} electrons, you could give every human on Earth a *billion* electrons each, and still have a some left over.

⁴The only other element that comes close to Li is beryllium (2974 mAh g^{-1}). Beryllium, however, is very toxic, scarce on Earth, and can be radioactive, why it is of little interest in commercial batteries [22].

aluminium (Al), and the external circuit. Current collectors connect to each electrode, enabling the transportation of electrons from the electrode materials to the external circuit. The external circuit provides a way to connect the cell to a device,

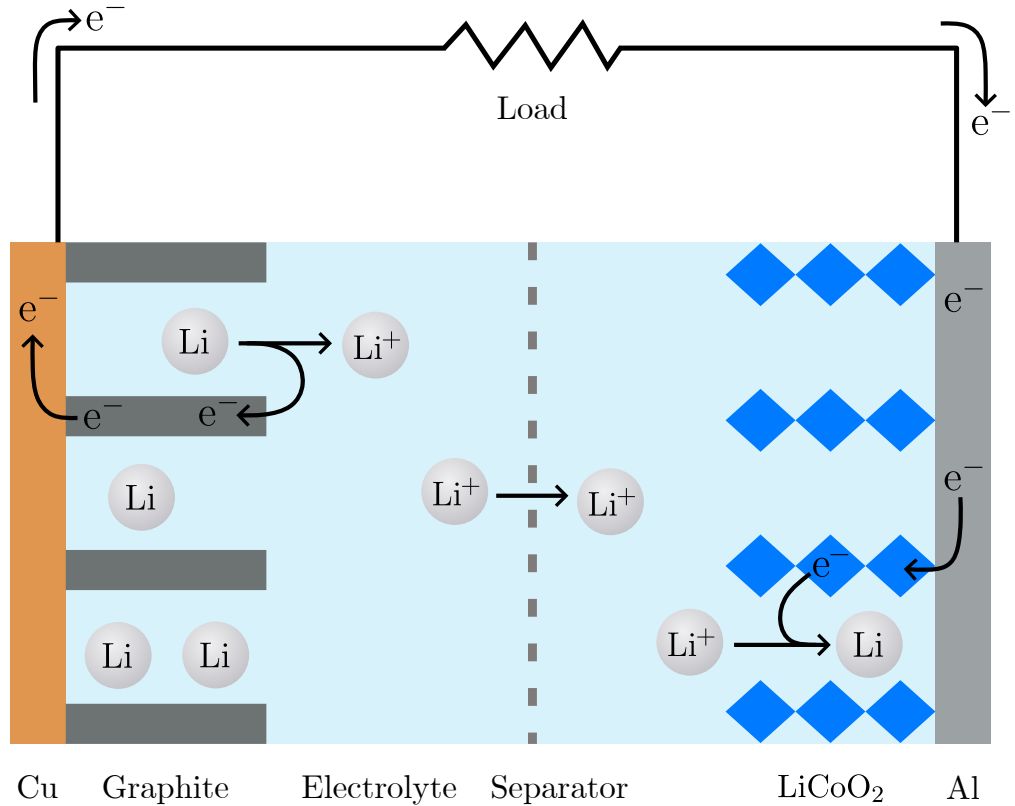


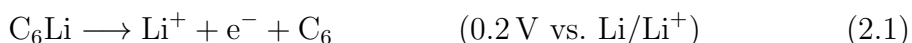
Figure 2.1. A schematic view of a cell in a LIB, showing the parts (not to scale) inside the cell casing. As an example, the electrodes are here graphite (each graphite layer is illustrated as gray rectangles) and LCO (blue rhombuses are CoO_2 -layers) which are commonly used in LIBs. The electrolyte (light blue background) enables transportation of ions, but not electrons, between the electrodes, and the separator (dashed gray line) keeps the electrodes from short-circuiting while letting Li^+ through. The current collectors, Cu (brown rectangle) and Al (gray rectangle), collect and transport the electrons to the outer circuit where the load is.

a load, thereby closing the circuit. The ions move between the electrodes through the electrolyte, and the electrons move from one electrode to the other through the current collectors and the external circuit. The structure of this cell can be compactly expressed as Gr/LCO (graphite/LCO).

Now that we know what the parts of a cell are and what general roles they play,

we will look at how the cell can store energy⁵ and release electrical energy as electrons. But before moving on, a short interlude is needed to introduce central concepts about voltage, oxidation, and reduction to explain what happens inside a cell. Voltage describes the energy available to do electrical work through motion of charge carriers, such as electrons. Specifically, voltage is energy per charge ($V = JC^{-1}$) and 1 V corresponds to 96.5 kJ per mole of electrons, which is comparable to energy changes in many electrochemical reactions [24]. While voltage describes energy per charge, it is measured as a *difference* in electrical potential energy. Thus, voltage must be given with respect to something. In electrochemistry, a common reference is the standard hydrogen electrode⁶ which is defined as 0.0 V with voltages being presented with respect to this. Another reference commonly used in battery research is Li/Li⁺, where the reaction $\text{Li} \rightleftharpoons \text{Li}^+ + e^-$ takes place on Li-metal. Moving on, chemical reactions can for our purposes be classified as either oxidation or reduction reactions. Oxidation means that a compound loses one or more electrons, while reduction means that one or more electrons is gained. These often occur simultaneously and are referred to as redox (reduction-oxidation) reactions.

Let us now look at the example of the cell in Figure 2.1 and its redox reactions. The cell is charged, meaning that Li are contained in the graphite. Since the cell is charged, energy has been put in to store the Li in the graphite, meaning that the Li have more energy in the graphite compared to what they had in the LCO. This extra energy can be extracted by discharging the cell by electrically connecting the electrodes through a load, as in Figure 2.1. From the charged state, Li in the graphite (C_6) can be released and become a Li-ion by giving away an electron according to



which is an oxidation reaction since the $C_6\text{Li}$ loses an electron, and the potential of this reaction is 0.2 V versus Li/Li⁺[25]. On the other side of the cell, the LCO can pick up a Li-ion and an electron according to



which is a reduction reaction since the LCO gains an electron and the voltage is 4.1 V versus Li/Li⁺[26]. Combining these gives



⁵For an explanation of how energy is stored and released in a cell, see [23].

⁶The standard hydrogen electrode consists in short of a piece of solid platinum on which the reaction $\text{H}_2 \rightleftharpoons 2\text{H}^+ + 2e^-$ occurs.

which is a redox reaction. In the example we have gone through, Li-ions move out from the graphite and into the LCO during discharge, while the electrons at the same time move from the graphite through the external circuit and load to the LCO. During charging, a voltage is applied to the cell and the arrows in the reactions above are flipped, indicating that reactions and movements of Li-ions and electrons are reversed.

With the example of the LIB in mind, the central concepts of cell potential, Gibbs free energy, and overpotential will now be introduced. The voltage difference between the two electrodes in a cell, called the cell voltage, is given by

$$E_{\text{cell}} = E_{\text{reduction}} - E_{\text{oxidation}} \quad (2.4)$$

where $E_{\text{reduction}}$ and $E_{\text{oxidation}}$ are the potentials of the reduction and oxidation reaction, respectively. For our example the overall redox reaction is given by Equation 2.3, and we get that $E_{\text{cell}}^{\text{Gr/LCO}} = 3.9 \text{ V}$ using the reduction and oxidation potentials from Equation 2.1 and Equation 2.2, respectively. This result, despite coming from a simple calculation, corresponds well with real LIBs which most often operate at 3.8 V [27]. Also, current I ($\text{A} = \text{Cs}^{-1}$), which describes the flow of charges, would in our example (approximately) describe how fast the redox reaction in Equation 2.3 occurs, with a higher current meaning more a higher reaction rate. In battery research, current is frequently expressed as a current density J (A cm^{-2}), where the current is divided by the area of the relevant electrode.

The cell voltage can also be obtained theoretically using the change in Gibbs free energy. Gibbs free energy G describes the maximum amount of work a closed system can do (that is not pressure-volume work). This is relevant because the change in Gibbs energy ΔG for a reaction dictates whether that reaction can occur spontaneously, if $\Delta G < 0$, or require external energy to happen, if $\Delta G > 0$. The voltage of a cell E_{cell} is related to ΔG and the charge passed through the cell nF according to

$$\Delta G = -nFE_{\text{cell}} \quad (2.5)$$

where n is the number of moles of electrons included in the redox reaction and $F = 96\,485 \text{ C mol}^{-1}$ is Faraday's constant (charge per mole of electrons) [24]. The negative sign takes into account that $E_{\text{cell}} > 0$ when a cell is discharging, and since the redox reaction happen spontaneously it must hold that $\Delta G < 0$. The change in Gibbs free energy will be used when discussion nucleation.

The final relevant concept introduced here is overpotential, which has to do with the potential of reactions. As stated, a given oxidation or reduction reaction occurs at some potential. That potential can be calculated theoretically and is therefore

called the theoretical equilibrium potential, $E_{\text{equilibrium}}$. The potential for which the reaction occurs in practice is E , and the overpotential η is then given by

$$\eta = E - E_{\text{equilibrium}} \quad (2.6)$$

which describes how far away from equilibrium the reaction actually takes place [24]. One reason that $E \neq E_{\text{equilibrium}}$ is that there is often an energy barrier that needs to be overcome in order for a reaction to occur. Also, a larger overpotential means there is a stronger driving force for the reaction, resulting in a larger current (higher reaction rate) in the case of an electrochemical cell. Overpotential will play an important role in nucleation, controlling both the size of Li nuclei and the number of nuclei per area [16].

We have now learned about the history of batteries, why Li is such a good candidate for high-energy batteries, gone through an example of the widespread LIB and simultaneously explained many of the fundamental concepts in an electrochemical cell, as well as concepts relevant to nucleation. Now, let us move on to one of the battery types that the next generation might use – the LMB.

2.3 Lithium-metal battery (LMB) example

A LMB basically a LIB in which the graphite (372 mAh g^{-1} for LiC_6) have been replaced by Li-metal (3862 mAh g^{-1}). As mentioned, this replacement can double the energy density [2] and drastically increase the specific energy of the cell [9]. An example of a LMB cell is shown during discharging in Figure 2.2, with LCO as the other electrode for easy comparison with the LIB cell in Figure 2.1. The replacement of graphite with Li-metal mean two main things. First, as stated, the specific capacity of Li-metal is almost ten times higher than that of lithiated graphite (LiC_6). Thus, more total capacity is achieved for the same electrode material. Secondly, the Li now needs to be stripped away from the Li-metal during discharging, and must then plate the surface (being deposited there) during charging. The plating can lead to several problems.

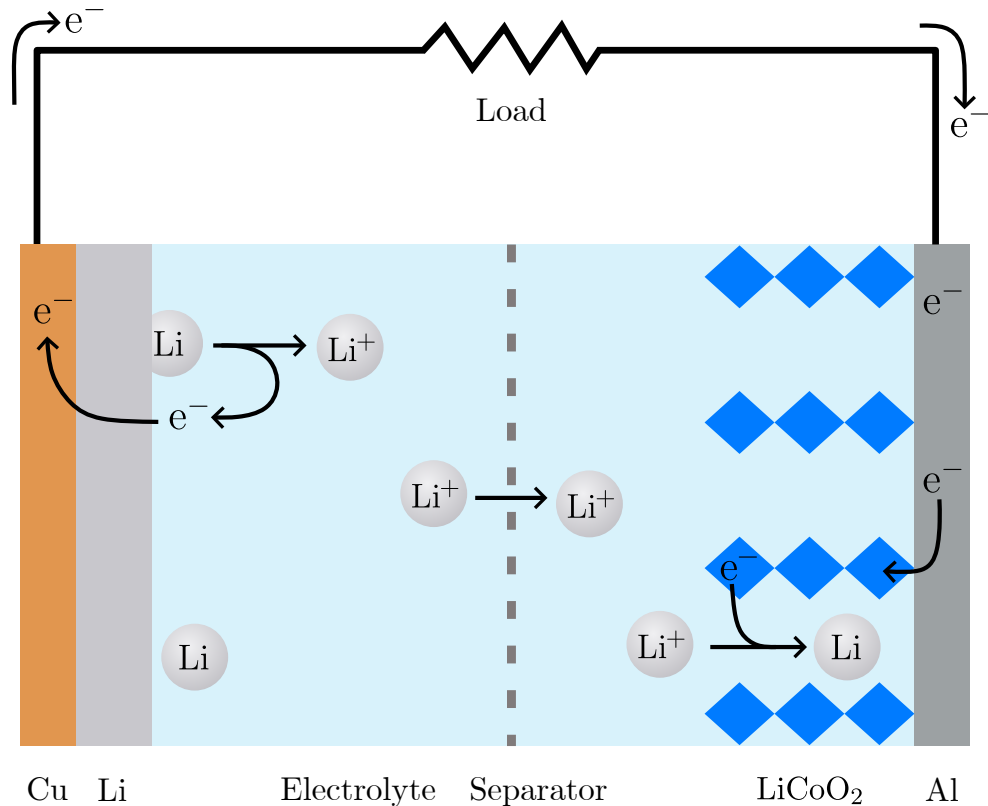


Figure 2.2. A schematic view of a cell in a LMB, showing the parts (not to scale) inside the cell casing. The parts are the same as in the case with the LIB cell (see Figure 2.1), with the graphite having been replaced by Li-metal.

2.3.1 Problems with non-uniform lithium deposition

The plating of Li on the Li-metal surface can cause several problems, as shown in Figure 2.3 [28]. First, the growing Li can penetrate the separator (not shown) and come into contact with the opposite electrode, in this example the LCO, causing a short-circuit in the cell. This is a serious safety risk as short-circuiting can lead to thermal runaway which can end in catastrophic failure where the cell explodes [28]. Secondly, "dead" Li can form. When fresh Li comes into contact with the electrolyte, irreversible reactions occur that forms a solid electrolyte interphase (SEI) layer. This SEI layer is electronically isolating and generally wanted on the electrode surface, as it passivates the surface (the SEI formation also stops once it reaches a certain thickness). However, when newly deposited Li comes into contact with the electrolyte, new SEI forms that can cover a piece of Li, and possibly making it lose contact with the Li below. This electronically isolated piece of Li is called "dead" Li. Creation of dead Li decreases the Coulombic efficiency [28]. Thirdly, the non-uniform deposited Li is porous, as opposed to closely packed like the pristine Li-metal, leading to a significant increase in volume of the electrode material. During many cycles, this repeated large increase and decrease in volume builds up mechanical stress which can cause the Li-metal to crack and break. Fourthly, since non-uniform growth of Li also increases the surface area exposed to the electrolyte, more (irreversible) side reactions occur between the Li and electrolyte. Amongst other things, this creates more overall SEI, decreasing the available Li for cycling, lowering the Coulombic efficiency [28]. All loss of active Li also leads to a decrease in the overall cell capacity.

As we have seen, there are several problems originating from non-uniform plating of Li that directly affects the cell performance through lowered Coulombic efficiency and loss of capacity over time. Finding ways to enable more uniform plating would eliminate, or at least lessen, these issues, thus improving the cell performance. To be able to reliably induce more favorable plating in LMBs, the first step during the deposition – nucleation – must first be well understood.

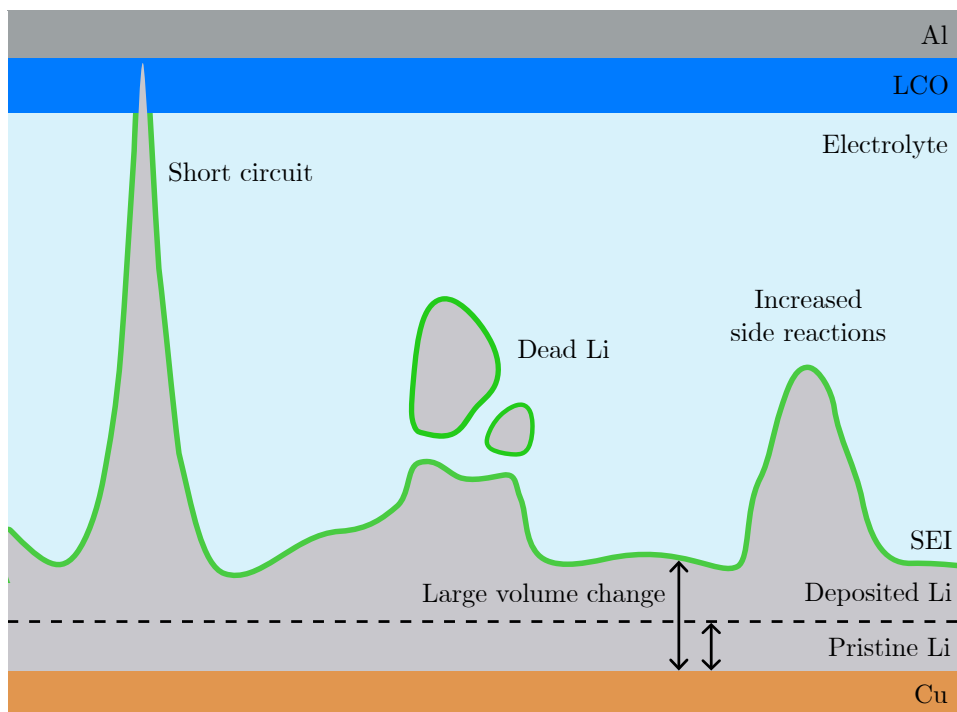


Figure 2.3. A schematic view of problems arising from non-uniform deposition of Li onto a pristine Li-metal surface in a LMB cell (not to scale). The main problems are short-circuiting the cell, formation of "dead" (electronically isolated) Li, large volume change, and increased rate of unfavorable (side) reactions. Short circuit occurs when the deposited Li penetrates the opposite electrode, here LCO. Dead Li is formed when a piece of Li becomes covered in a SEI layer (green outline of the deposited Li) and is therefore electronically isolated. Large volume change happens due to the deposited Li being more porous than the pristine Li. Increased side reactions is due to the increased surface area from the non-uniform deposited Li, providing more sites for side reactions. Figure inspired by [28].

3

Nucleation

A key concept in this work is nucleation. Nucleation is the first step in forming a new phase or structure, which in this work means forming solid Li from a solution containing Li-ions. After having formed Li nuclei with a size large enough to be thermodynamically stable, the nuclei will continue to grow if supplied with more Li. In this section, the steps of nucleation are first described which are then followed by homogenous nucleation theory. Homogenous nucleation theory provides important concepts for understanding nucleation. Lastly, the specific scientific questions this work aims to answer are presented.

3.1 Steps during nucleation and growth

Here we consider nucleation of Li from an electrolyte containing Li^+ onto a Cu surface. Nucleation consists of several steps, shown in Figure 3.1. Following one (solvated) Li-ion, the first step is mass transport of the ion through the electrolyte and SEI layer (not shown) to the Cu surface. Next is charge transfer, where the Li-ion is reduced (gains an electron) and becomes a Li atom which can then be adsorbed to the surface. Finally, adsorbed Li combines into a cluster with other adsorbed Li atoms and forms nuclei. The growth of these formed nuclei occurs in the same way, where additional Li-ions are reduced and adsorbed to the existing nuclei. Note that for nucleation to occur, an energy barrier needs to be overcome. The existence of this energy barrier can be seen in a deposition curve.

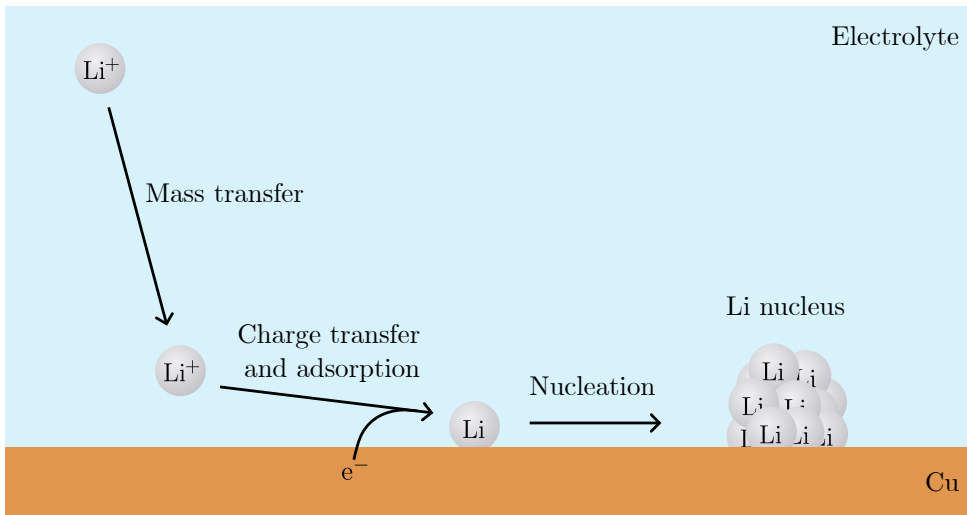


Figure 3.1. Steps during nucleation of Li. A Li^+ gets transported through the electrolyte towards the Cu substrate. Then, an electron reduces the ion to a Li atom, which then adsorbs onto the surface. Nucleation occurs when many Li atoms cluster together, forming a nucleus. Figure inspired by [29].

3.2 Deposition curve in a cell

Here we consider deposition of Li in a cell with Li-metal as one electrode and Cu as the other. The characteristic deposition curve is shown in Figure 3.2 as voltage of the Cu substrate versus the Li as function of charge passed. A certain driving force, overpotential, is needed to start the nucleation process on the bare Cu. This is seen as the sharp drop in potential, which reaches its lowest value at η_n (subscript n for nucleation). At this region of the curve, nucleation occurs. Once nuclei have formed, the voltage increases and reaches a plateau at η_p (subscript p for plateau). At this region of the curve, nuclei grow. Below the curve, a schematic illustration of Li deposition on the Cu surface is shown. The left-hand side shows that a voltage difference between the electrodes gives rise to an electric field, which exerts a force on positive charges like Li^+ in the direction of the field lines. Li atoms from the Li electrode can release their electron and move out into the electrolyte as Li^+ . The electric field drives mass transport of Li^+ towards the Cu where the Li^+ can recombine with electrons, forming Li nuclei (by the steps presented in Figure 3.1). Hence, the charge passed through the outer circuit indicates the amount of deposited Li. Note that the overpotential for nucleation is larger in magnitude than the overpotential for growth, $|\eta_n| > |\eta_p|$. In other words, the energy barrier is different for nucleation and growth. This can be modelled theoretically with nucleation theory.

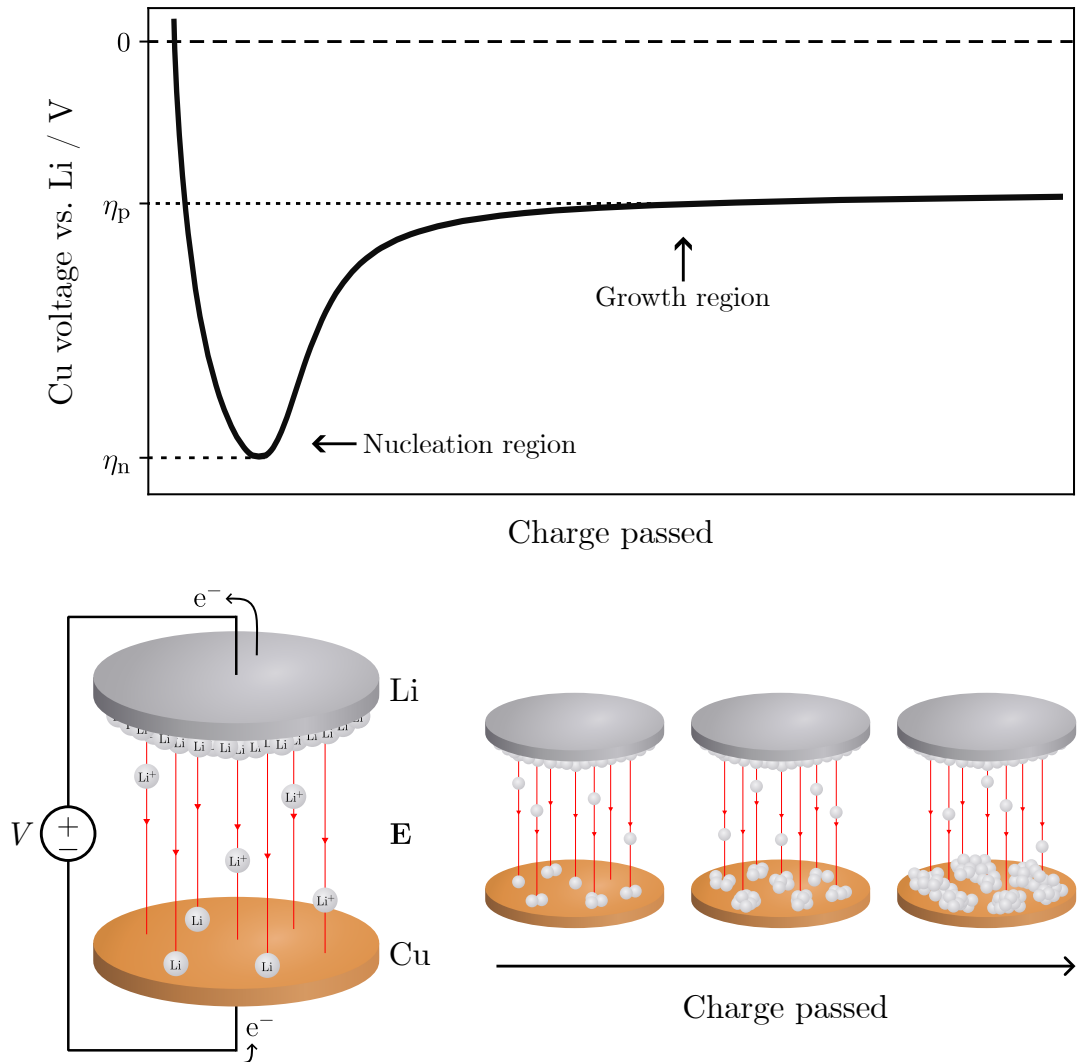


Figure 3.2. Top: Characteristic deposition curve showing voltage of the Cu substrate versus Li as function of charge passed. The overpotential for the nucleation region η_n and for the plateau (growth) region η_p are marked. Bottom: Schematic illustration of Li deposition on Cu. A voltage difference V between the electrodes induces an electric field \mathbf{E} (red lines with arrows), exerting a force on positive charges (like Li^+) in the direction of the field lines. The \mathbf{E} drives Li^+ toward the Cu, where the ions can recombine with electrons and form Li atoms on the surface. The deposited Li atoms first form nuclei (nucleation region), which then grow as more charge get passed (growth region).

3.3 Homogenous nucleation theory

Nucleation theory starts with thermodynamics, specifically the change in Gibbs free energy. In general terms, when a new solid phase is formed from a solution, there is a cost in energy for creating surface area ($\Delta G_{\text{surface}} > 0$) and at the same time a gain in energy for creating bulk ($\Delta G_{\text{bulk}} < 0$). In the case of homogenous nucleation, the change in Gibbs free energy for forming a nucleus can be written

$$\begin{aligned}\Delta G &= \Delta G_{\text{surface}} + \Delta G_{\text{bulk}} \\ &= A\gamma + V\Delta G_V \\ &= 4\pi r^2\gamma + \frac{4}{3}\pi r^3\Delta G_V\end{aligned}\quad (3.1)$$

where A is the surface area created, γ is the surface energy of the interface between the two phases, V is the volume of the nucleus, ΔG_V is the change in Gibbs energy per created volume, and in the last line we assume that the nucleus is spherical with radius r . The overpotential $\eta = \eta_n$ for nucleation is related to ΔG_V as

$$\Delta G_V = -\frac{F|\eta|}{V_m} \quad (3.2)$$

where F is Faraday's constant and V_m is the molar volume of the element creating the nucleus [16]. The expression in Equation 3.1 is shown in Figure 3.3 as function of r . It is the cost in energy associated with $\Delta G_{\text{surface}}$ that gives rise to the energy barrier $\Delta G_c = \Delta G(r_c)$ for nucleation. Here, r_c is the critical radius of nucleation, the radius for which the nucleus becomes thermodynamically stable. As long as the size of the nucleus is $r < r_c$, it is unstable since the system needs to expend energy to form the nucleus. But once $r > r_c$, the nucleus grows spontaneously since this lowers the Gibbs free energy of the system. This can be shown by considering the change in Gibbs free energy for the addition of one particle to the nucleus. Adding one particle means a small increase dr to the radius and Gibbs free energy changes as $\Delta G_{\text{particle}} = \Delta G(r + dr) - \Delta G(r)$. If $\Delta G_{\text{particle}} < 0$, the Gibbs free energy is lowered and the nucleus grows spontaneously. Thus, the condition $\Delta G(r + dr) < \Delta G(r)$ determines r_c which can be derived by setting the derivative of Equation 3.1 equal to zero and solving for $r = r_c$,

$$\begin{aligned}\frac{\partial}{\partial r}\Delta G &= (8\pi r\gamma + 4\pi r^2\Delta G_V) \Big|_{r=r_c} \\ &= 8\pi r_c\gamma + 4\pi r_c^2\Delta G_V \\ &= 4\pi r_c(2\gamma + r_c\Delta G_V) \stackrel{!}{=} 0\end{aligned}$$

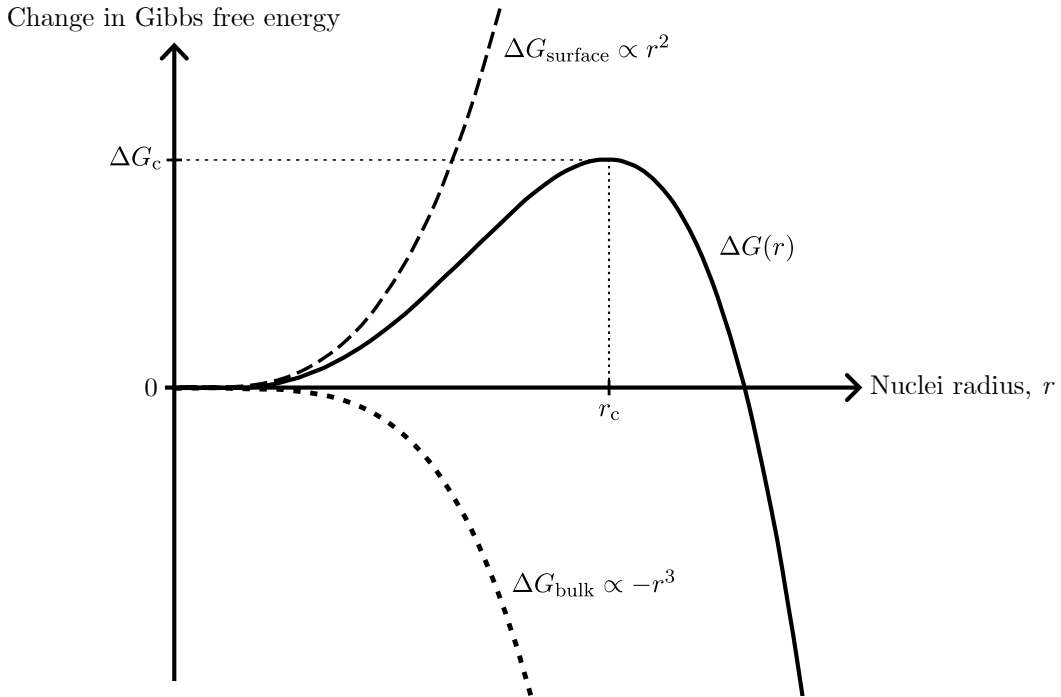


Figure 3.3. Characteristic plot of $\Delta G(r) = \Delta G_{\text{surface}} + \Delta G_{\text{bulk}}$ where $\Delta G_{\text{surface}} \propto r^2$ and $\Delta G_{\text{bulk}} \propto -r^3$ for a spherical nucleus, as function of nucleus radius. At the point where growth of the nucleus lower the overall energy of the system, when $\Delta G(r + dr) < \Delta G(r)$, a critical radius r_c is reached. Once $r > r_c$, the nucleus will grow spontaneously since this lowers the Gibbs free energy of the system. The cost in energy for the surface $\Delta G_{\text{surface}}$ induces an energy barrier equal to $\Delta G_c = \Delta G(r_c)$ that needs to be overcome for nucleation to occur.

which, ignoring the solution $r_c = 0$, gives

$$r_c = -\frac{2\gamma}{\Delta G_V}.$$

By using Equation 3.2 this results in

$$r_c = \frac{2\gamma V_m}{F|\eta|} \quad (3.3)$$

from which we see that the size of the nuclei is inversely proportional to the overpotential, $r_c \propto \eta^{-1}$. This can also be seen from the fact that the energy barrier for nucleation ΔG_c is dependent on the overpotential $|\eta|$ (Equation 3.1 and Equation 3.2). Hence, when the overpotential is increased the energy barrier decreases, which in turn changes r_c . This means that the size at which nuclei becomes stable is dependent on η , as described by Equation 3.3. Moreover, one should expect

not only that the size is dependent on η but also that the number of nuclei per area changes as well (given the same amount of deposited Li). One can in fact show¹ that the areal nuclei density N , number of nuclei per area, is proportional to the overpotential to the third power, $N \propto \eta^3$. These relations, $r_c \propto \eta^{-1}$ and $N \propto \eta^3$, influence the nuclei distribution as function of overpotential, as shown in Figure 3.4. These theoretical relations have been supported by experiments [16].

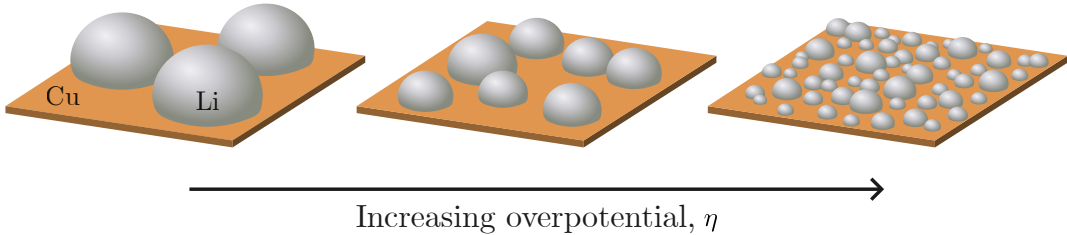


Figure 3.4. When the overpotential increases, the size of the Li nuclei decreases as $r_c \propto \eta^{-1}$ while the areal density increases as $N \propto \eta^3$. Figure inspired by [16].

The presence of a substrate means that it is heterogeneous, and not homogenous, nucleation which actually takes place in a LMB. Heterogeneous nucleation theory can model nucleation on a flat surface by taking more parameters into account with increasing complexity. However, the case of homogenous nucleation provides the essential concepts for nucleation while being simpler to understand. We have seen that it is the cost in energy for creating surface area, as opposed to the gain in energy for creating bulk, which leads to an energy barrier for nucleation. This can be seen in the deposition curve (Figure 3.2), where a large $|\eta_n|$ is required for nucleation, but a smaller $|\eta_p|$ is sufficient for subsequent growth. This is explained as the surface term in ΔG scaling as r^2 , while the bulk term scales as $-r^3$. Having provided a fundamental understanding of the nucleation process through nucleation theory, the aim of this work can now be more precisely specified.

3.4 Specific scientific questions in this work

//***to be written ***

¹Given that $r \propto \eta^{-1}$, we can show that the areal nuclei density is proportional to the third power of the overpotential, $N \propto \eta^3$. First, let n be the number of nuclei, V be the total deposited volume, r be the radius of the nuclei, and A be a fixed area on which N is calculated. Next, we have $V = nr^3$ because the total volume deposited is the number of nuclei times their volume (assuming spherical nuclei), which gives $n = V/r^3$. Since we seek $N = n/A$, we put together the relations above to get $N \propto n \propto r^{-3} \propto \eta^3$, where $r \propto \eta^{-1}$ was used in the final step. Finally, we arrive at the conclusion that $N \propto \eta^3$, in agreement with [16].

- Is the nucleation influenced by other reactions in the cell (such as SEI formation)? Can this be influenced using different cell configurations?
- Is the nature of electrochemical nucleation more instantaneous (all nuclei form first and then all grow) or more progressive (new nuclei can form during the growth of earlier nuclei)? Under what conditions is the nucleation more instantaneous or progressive?
- How does pressure influence the nucleation process?
- How does current density influence the nucleation process? (J is known to affect η , which affects r and N , but does J also influence whether the nucleation is more instantaneous/progressive?)
-
-

(från Josefs mail):

In which steps does Li growth occur in the very early stages and why?

* Do all nuclei grow at the same time? Or do some nuclei only form and then stop/get passivated?

How can the nucleation process be influenced?

How do we image the nuclei accurately?

* How stable are Li nuclei? * Which experimental conditions are necessary to consider in a nucleation study? * How can influence from corrosion and side reaction be minimized in nucleation studies?/How can we wash electrodes?)

What influence does a change in nucleation behavior have for the performance of the cell? (mostly CE)

4

Methods

This section first shows the material preparation and the different types of cell configurations used. Then, the setup and protocols used for electrochemical cycling of the cells are described, followed by a section focusing on the scanning electron microscope (SEM). Lastly, the data analysis of the obtained SEM images and cycling data is explained.

4.1 Material preparation

4.1.1 Electrode materials

The electrode materials used were Cu (Goodfellow, 0.1 mm thick sheet, 99.9 % purity) and Li (Chemetall, 0.2 mm thick). The Li was prepared inside the argon-filled glove box by punching out circular pieces with a diameter of 5 mm. The preparation of Cu took place outside the glove box. Preparation began with polishing, where each Cu sheet were polished using grinding paper placed on a turn table (Buehler Beta grinder-polisher), see Appendix A.1 for details. The following silicon carbinate grinding papers from Beuhler were used: P1200, P2500, and P4000, in order of polishing from coarser to finer. This resulted in a mirror-like finish for the Cu sheet (see Figure 4.1). As shown in Figure 4.1, a puncher was used to produce circular disks of Cu with diameter 10 mm from the polished sheet. Next followed the washing procedure of the circular disks. A ultrasonic cleaner (Fisherbrand Easy) was used, where each Cu piece was placed polished side up in its own glass beaker to avoid scratches during the washing procedure. Each glass beaker containing one Cu piece was filled with acetone and put into the ultrasound cleaner for 10 min at room temperature. The acetone was thereafter poured out, and each glass beaker filled with isopropanol for another ultrasound clean for 10 min at room temperature. The Cu disks were then dried by pouring out the solvent and letting the remaining solvent evaporate, after which the disks were placed in a glass beaker and finally transferred into the glove box.

4.1.2 Electrolytes

The main electrolyte used was lithium bis(fluorosulfonyl)imide (LiFSI) salt in the solvent 1,2-dimethoxyethane (DME). The LiFSI salt was dried in an oven (Büchi B-580) at 80 °C for at least 24 h under vacuum. To remove water molecules from the solvent, the DME was put into a glass vial together with molecular sieves with pore size 3 Å. The molecular sieves had previously been dried in the oven at 230 °C for 24 h under vacuum. The DME soaked the molecular sieves for at least 24 h and the DME was then pushed through a filter (Acrodisc PSF with 0.45 µm pore size) before use.

The main electrolyte had a 4 mol L^{-1} concentration of LiFSI salt in DME. This concentration was achieved by using a mole ratio of 1.4/1 (DME/LiFSI) [13]. The two other electrolytes used were lithium hexafluorophosphate (LiPF_6) and an ionic liquid (IL). The LiPF_6 consisted of 1.0 mol L^{-1} LiPF_6 salt in ethylene carbonate (EC) and ethyl methyl carbonate (EMC) with ratio 1/1 (EC/EMC). The LiPF_6 electrolyte was taken as bought from Sigma-Aldrich. The IL consisted



Figure 4.1. The puncher was used to punch circular disks with diameter 10 mm out of the polished Cu sheet. One 70 mm × 70 mm sheet resulted in about 30 Cu disks.

of lithium bis(trifluoromethanesulfonyl)imide (LiTFSI) in the electrolyte 1-Butyl-1-methylpyrrolidinium bis(fluorosulfonyl)imide (BMPyrrFSI) with mole ratio 1/4 (LiTFSI/BMPyrrFSI). The LiTFSI had been dried at 80° for 24 h in vacuum. Both the LiTFSI and the BMPyrrFSI were bought from Solvionic. The preparation of the electrolytes and the DME was carried out in a glove box filled with argon gas.

4.2 Cell configurations and assembly

The cell configuration includes the geometry, choice and volume of electrolyte, choice of separator, and pressure between the electrodes. Here, the assembly process of the coin cell (C-cell), the Swagelok-type two-electrode cell (I-cell), and Swagelok-type three-electrode cell (T-cell) are described. The C-cell is a common configuration, although the pressure between the electrodes can be unevenly distributed [30]. On the other hand, the I-cell can be built with a known, and hopefully more even, pressure between the electrodes compared to the C-cell. Lastly, while the T-cell can be built without pressure between the electrodes, it also enables measurement with a reference electrode. All cells were assembled inside an argon-filled glove box with oxygen levels below 4 ppm and water levels below 0.01 ppm.

4.2.1 The coin cell (C-cell)

Figure 4.2 shows the parts that make up a C-cell and the assembly. The main parts of the cell are Li, separator and electrolyte, and Cu. The can, gasket, and cap keep the main parts in place and seals the cell shut, while the wave spring applies pressure between the electrodes. For each cell, Wellcos 2032 type cell parts were used and 25 μL of electrolyte was added to one separator using a micropipette during assembly.

Specifically, most C-cells were assembled with 25 μL electrolyte of 4 mol L^{-1} LiFSI in DME added to one Celgard 2400 separator. However, when comparing electrolytes one cell instead had 25 μL electrolyte of 1 mol L^{-1} of LiPF₆ in 1/1 ratio of EC/EMC added to one Celgard 2400 separator, and one cell had 25 μL electrolyte of IL added to one Whatman glass fiber separator (because the IL did not wet the Celgard 2400 separator).



Figure 4.2. The parts of a C-cell is shown to the left. Electrolyte is added to the separator during assembly. The parts are first put into the can as shown, and the cap is first pushed into the gasket by hand, resulting in the C-cell to the upper right. The assembly is then finalized by bending the can walls inwards using a hand-turned press (not to scale), ensuring a tight fit between the can, gasket, and cap. The closed C-cell is shown below the hand-turned press.

4.2.2 The Swagelok two-electrode cell (I-cell)

This cell is a Swagelok-type¹ two-electrode cell, as it has two electrodes which in this case will be metal rods connecting to the Li and Cu. The parts of the I-cell are shown in Figure 4.3. Though most of the parts are stainless-steel, the metal rods are physically separated from the main body by virtue of the Swagelok sealing rings (being non-conductive), preventing a short circuit between the Li and Cu. For each assembly, 25 μL electrolyte of 4 mol L⁻¹ LiFSI in DME was added to one Celgard 2400 separator using a micropipette during assembly.

A spring with measured spring constant (520 ± 14) N m⁻¹ was used in each cell to apply pressure between the Li and Cu. The pressure was calculated by measuring the total length of each assembled I-cell (from which the compression length of the spring could be computed), and taking the area of interest to be that of the punched Li 5 mm in diameter. This resulted in a pressure equal to (267 ± 16) kPa, or (2.64 ± 0.16) atm, for all assembled I-cells. The uncertainty in the pressure comes from error propagation of the quantities used to calculate the pressure, also taking into account different total lengths of the assembled cells.

¹Swagelok refers to the way two conical plastic rings are used together in order to achieve a leak-tight seal, here between the steel rods and the walls of the cell. The rings are called the front and back ferrule, and will together be referred to as Swagelok sealing rings for simplicity.

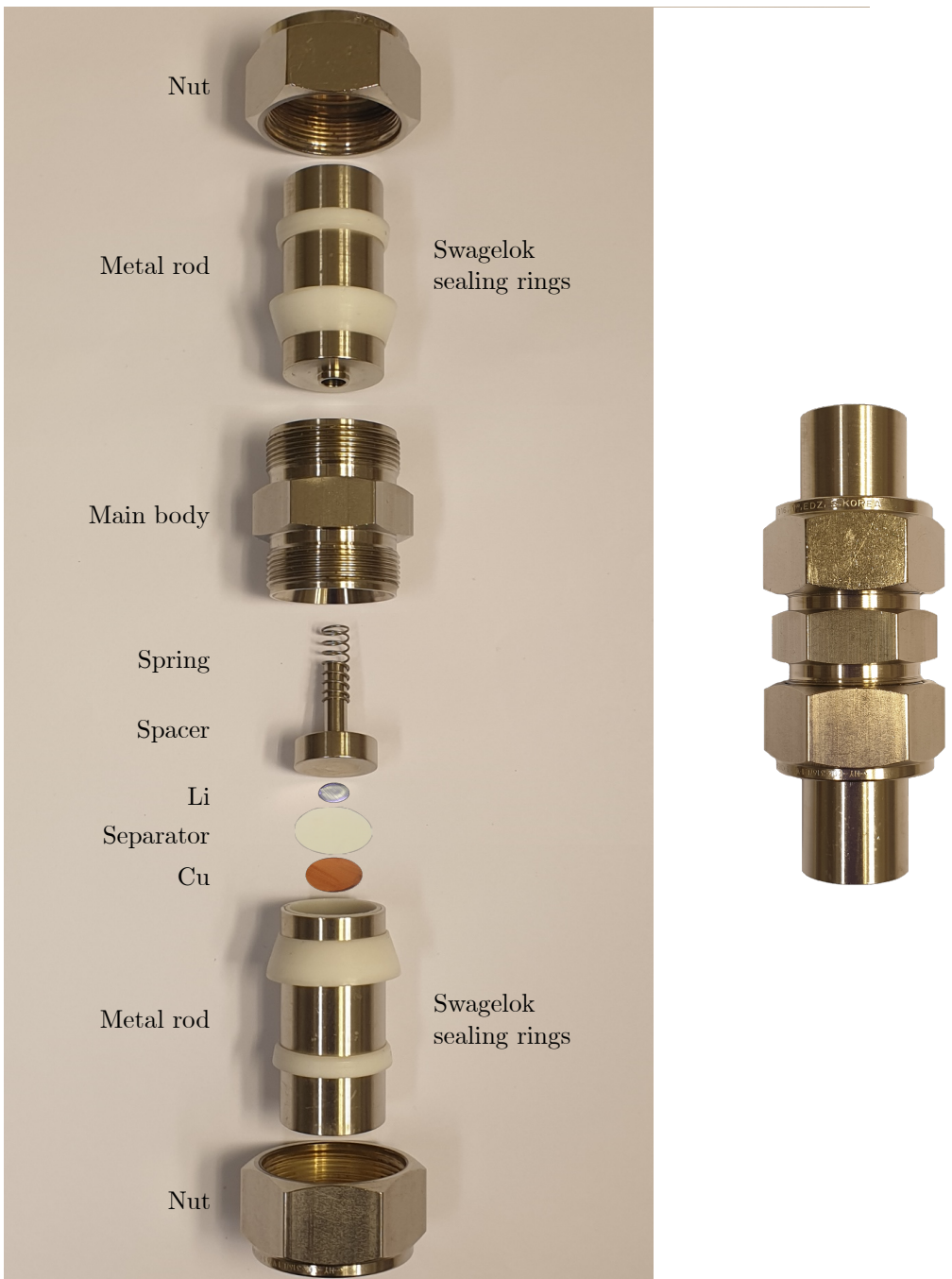


Figure 4.3. Parts of the I-cell. First, the Cu, separator, electrolyte (added to the separator during assembly), and Li are put into the lower metal rod in that order. The rest of the cell is then assembled by moving the other parts inwards and tightening the nuts onto the main body. Tightening of the nuts achieves a leak-tight seal thanks to the Swagelok sealing rings. The spring, being compressed during assembly, applies pressure to the Li and Cu. The assembled I-cell is shown to the right.

4.2.3 The Swagelok three-electrode cell (T-cell)

For a cell without pressure between the electrodes, a T-cell can be used. In this case, a custom-built Swagelok-type T-cell made of polyether ether ketone (a plastic with high chemical resistance) and stainless-steel rods was used. The main body of the cell has a hollow T-part, allowing three metal rods to be inserted. The parts of the T-cell is shown in Figure 4.4. The 1 mm polypropylene (PP) horseshoe-shaped spacer used was made from a 1 mm thick sheet of PP, see Appendix A.2 for details. The spacer prevents physical contact between the Li and Cu, meaning there is no applied pressure between the two electrodes. For each assembly, 75 μL electrolyte of 4 mol L^{-1} LiFSI in DME was added using a micropipette (no separator was used). In the case when the full three-electrode setup was used, the third (last) metal rod was assembled with Li, as well as a glass fiber separator (**manufacturer**) and extra electrolyte to wet the separator.

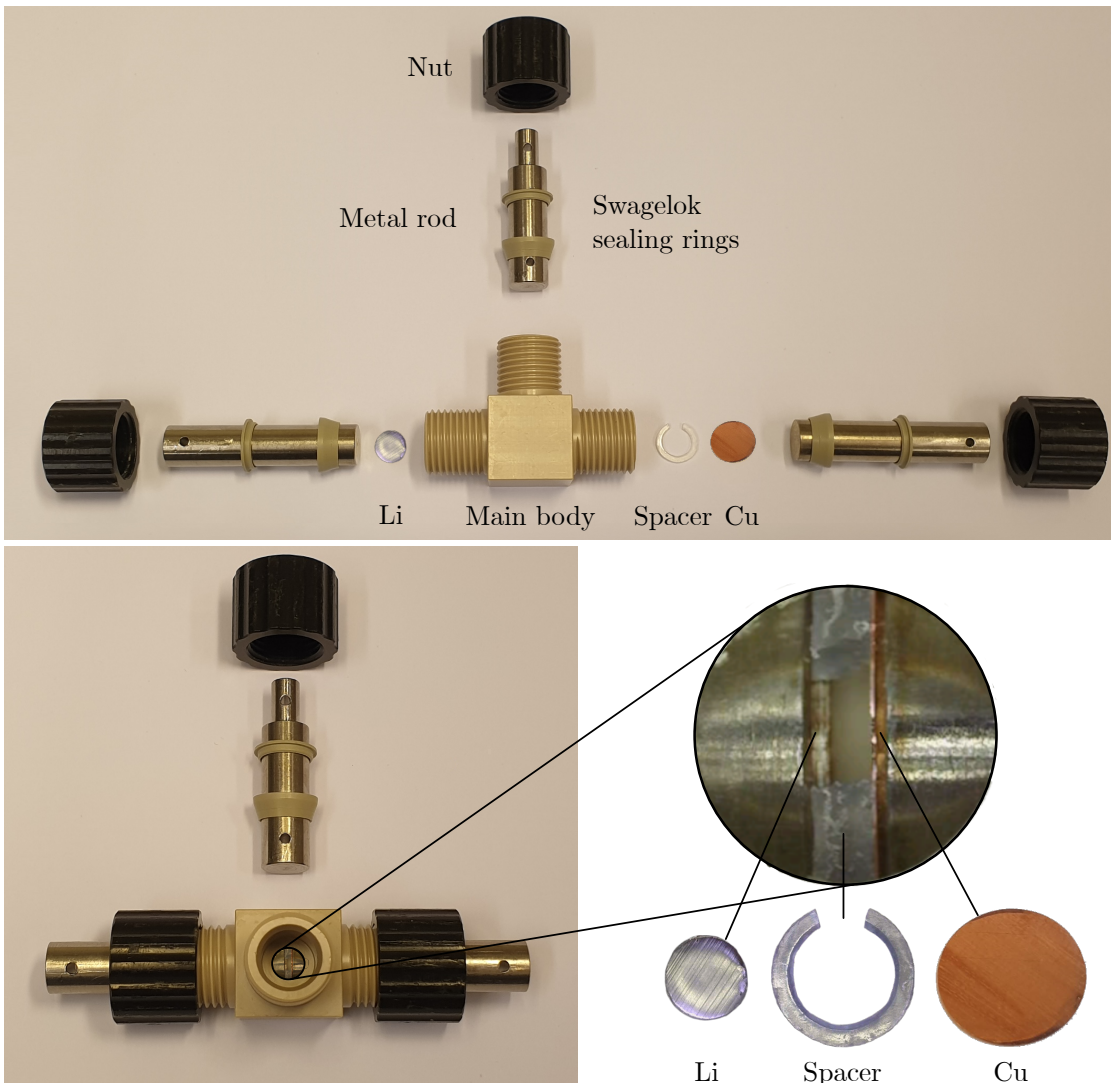


Figure 4.4. Parts of the T-cell. First, the metal rods on the sides are inserted along with the Li, spacer, and Cu. Then, the Swagelok sealing rings are mounted on the metal rods and the leak-tight seal is achieved by tightening the nuts onto the main body. Next, the electrolyte is added through the opening in the spacer, as shown in the magnification. The assembly is finalized by inserting the third metal rod and tightening the last nut. The magnification shows that the spacer creates a gap between the Li and the Cu, meaning there is no applied pressure between the electrodes.

4.3 Electrochemical cycling of the cells

Once the cells were assembled, they were attached to an instrument and subjected to a cycling protocol. For the samples to be measured in SEM, the Scribner Associates 580 Battery Test System was used for cycling of C-cells. For all other measurements, the VMP3 Multichannel Potentiostat (Biologic) was used. Moreover, the C-cells and I-cells were cycled outside the glove box at ambient conditions, while the T-cells were cycled inside the glove box. The cycling protocol is described below, as well as the sample preparation after cell disassembly for the measurements in SEM.

In general terms, the goal for the cycling protocol was to first see an indication that the cell had been assembled correctly, then to passivate the Cu surface, and finally to deposit Li on the Cu. The first point, seeing that the cell was not obviously bad, was done by having a period when the open-circuit voltage (OCV) is measured. OCV is the potential of the cell when no load is connected to the cell. In the case of the Li/Cu cell, a good OCV means a cell potential of about (2.8 ± 0.2) V.² The second point, to passivate the substrate, was achieved by forming the SEI through a constant voltage (CV) hold. When the voltage is held constant, the current is allowed to change freely. It was therefore possible to use the current as an indicator of how passivated the substrate was. When a low current is reached, the side reactions (such as forming the SEI) must occur slowly, and the substrate is thus more passivated. The third point, deposition of Li, was performed by applying a constant current (CC) in the direction such that Li is forced to move to the Cu. If the OCV was positive, then the deposition current should be negative. All in all, the cycling protocols were made up of three main parts, the OCV checking the cell status, followed by the CV hold forming the SEI, and finally the CC depositing Li.

4.3.1 Cycling protocol for SEM images

For the measurements in SEM, the cycling protocol was as follows. First 1 min of OCV, then 15 min of CV at 0.010 V, and finally CC deposition using $J_{\text{deposition}} = 1 \text{ mA cm}^{-2}$ and various $t_{\text{deposition}}$. The length of $t_{\text{deposition}}$ affects the total deposited areal capacity (mAh cm^{-2}) for a given $J_{\text{deposition}}$.

²The convention here was to connect the cell to the instrument such that the OCV of the cell was positive.

4.3.2 Cycling protocol for electrochemical measurements

For the electrochemical measurements, the cycling protocol was as follows. First 1 min of OCV, then a CV hold at 0.010 V until a cutoff value $I_{\text{SEI-cutoff}}$ was reached, then a short OCV period for 0.1 s, and finally CC deposition using $J_{\text{deposition}}$ with a total deposited areal capacity of $500 \mu\text{A h cm}^{-2}$. Having a fixed time of SEI formation by a CV hold at 0.010 V resulted in different amounts of passivation for the different cell configurations. Therefore, the cutoff value $I_{\text{SEI-cutoff}}$ was used in order to have more control over the ratio between the current of the reactions during formation of SEI and the current during deposition. The purpose of the added, second, OCV was only to allow the software of the Biologic to change the current range during measurement when switching from the SEI formation (low current) to the Li deposition (in some cases much higher current). Optimally, the second OCV should not be present, although its short duration is unlikely to have any significant effect on the results.

When creating the cycling protocol in the Biologic software, the data acquisition could be controlled for the different parts of the protocol. Acquisition of a data point was made each time either the current or potential changes by some value, $\Delta I_{\text{acquisition}}$ or $\Delta E_{\text{acquisition}}$, or some time had passed since the last acquisition, $\Delta t_{\text{acquisition}}$. During the OCV part, $\Delta t_{\text{acquisition}} = 10 \text{ s}$. For the SEI formation part, $\Delta I_{\text{acquisition}} = 50 \mu\text{A}$ and $\Delta t_{\text{acquisition}} = 10 \text{ s}$. During this part of the protocol, the current range was set to automatic, meaning that the range of currents that the instrument could accurately measure automatically changed as the magnitude of the current during the SEI formation changed. For the part with deposition of Li, $\Delta E_{\text{acquisition}} = 1 \text{ mV}$ and $\Delta t_{\text{acquisition}} = 10 \text{ s}$. The current range was in this part set to a value corresponding to $I_{\text{deposition}}$.

4.3.3 Sample preparation for SEM

For the samples to be measured in SEM, each cell was disassembled and the Cu washed inside the glove box. The washing procedure consisted of immersing and letting the Cu rest in fresh DME for 1 min. The Cu was then carefully touched edge on to a napkin in order to drain the DME from the surface. Next, the washed and dried Cu was attached by adhesive Cu tape to the SEM stage (a metal cylinder). Finally, when this procedure was done for the samples to be measured at that particular time, the SEM stage was put into the transfer chamber which was then closed inside the argon-filled glove box. The next time the transfer chamber was opened was under vacuum while transferring the SEM stage into the SEM instrument.

4.4 Electron microscopy

Optical microscopes use visible light to image objects, but there is a limit to how small of an object can be resolved. The limit is given by the Abbe diffraction limit which gives the spatial resolution of a microscope as

$$r = \frac{\lambda}{2n \sin \theta}$$

where r is the minimum distance between two resolvable points (the resolution), λ is the wavelength of the particle used to image the object (commonly photons or electrons), n is the refractive index of the media surrounding the imaged object, and θ is half the opening angle to the imaging lens [31]. Based on the Abbe diffraction limit, optical microscopes can at best resolve two points about 0.3 μm apart.³ However, the resolution improves with shorter wavelength, and it is possible to reach shorter wavelengths by using electrons instead of visible photons.⁴ That is the idea of an electron microscope, in which a spatial resolution of 0.001 μm can be achieved [32]. An electron microscope is favorable in this study for adequate resolution, as the size of deposited Li particles can be about 1 μm [16].

4.4.1 Scanning electron microscope (SEM)

The main components of a SEM are shown schematically in Figure 4.5. All parts of the SEM are enclosed in a vacuum chamber to avoid both contaminating the sample and having the electron beam deflected by other molecules. Starting from the top, the electron gun provides free electrons, for example by thermal emission of electrons from a heated tip of tungsten. A positively charged ring (the accelerator) then attracts and thereby accelerates the negatively charged electrons downwards in Figure 4.5, towards several electromagnetic lenses. The electromagnetic lenses generate magnetic fields (by passing current through coils of wire) which focuses the electrons to a fine beam with a small diameter. A small electron beam diameter means high spatial resolution. Electrons in the beam are called primary electrons and interact with the atoms in the sample, which can cause electrons to be emitted from the sample. Such emitted electrons are called secondary electrons (SEs) and

³ Assuming, as an example, that $n \sin \theta = 1$ (this is equal to numerical aperture, with a value around 1 for lenses in air) and green light, $\lambda = 500 \text{ nm}$.

⁴ Let us compare the wavelength of electrons and visible photons. Combining kinetic energy $E_k = mv^2/2 = p^2/(2m)$, where m is mass, v is speed and p is momentum, with the de Broglie wavelength $\lambda = h/p$, where h is Planck's constant, we get $\lambda = h/(2mE_k)^{1/2}$. Now, an electron accelerated to 10 keV, a standard acceleration voltage in a SEM, would have a wavelength of 0.012 nm. Compare that to visible photons with wavelengths between 400 nm and 700 nm. Clearly, electrons results in a significantly shorter wavelength compared to using visible photons.

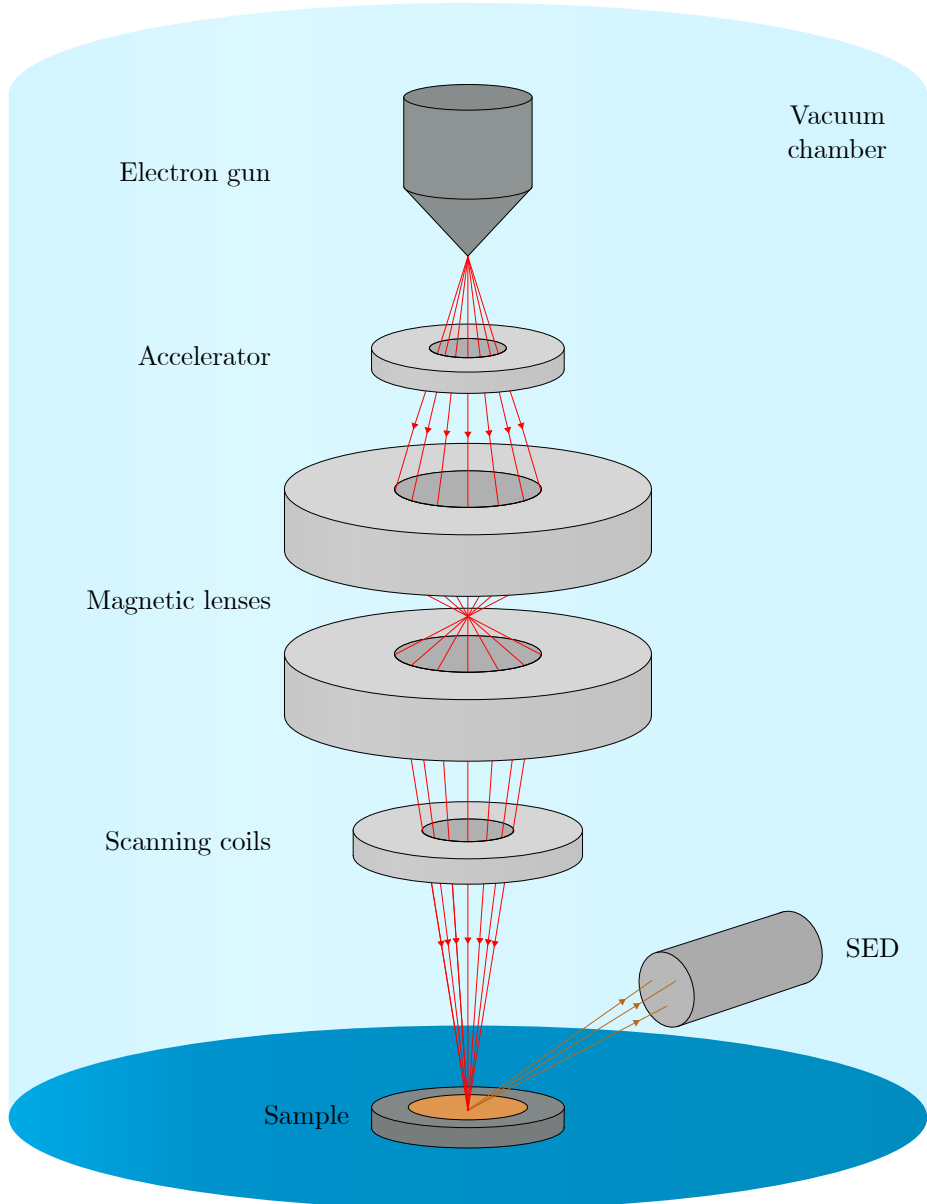


Figure 4.5. Schematic overview of the main components of a SEM. The electron gun ejects electrons (represented as solid red lines) that get accelerated by the accelerator. The electrons are then focused to a small point by the magnetic lenses. The scanning coils raster scans the beam over the sample, resulting in ejected electrons that are finally measured using detectors, for example using a secondary electron detector (SED). The final imaged is obtained through software where a pixel image is build up from the detector signal during the raster scan.

are measured using a secondary electron detector (SED). Closest to the sample are the so-called scanning coils. These coils deflect the electron beam sideways in a controlled manner, allowing the electron beam to be raster scanned across the surface of the sample. All the probed spots (pixels) during the raster scan come together to form a black and white image, where the intensity of each pixel is proportional to the signal from the SED (white means high signal and black means low signal).

Images were obtained using a SEM (PHI 700 scanning Auger nanoprobe) with an acceleration voltage of 10 kV and a beam current of 10 nA for the C-cell samples and 5 nA for the T-cell samples.

4.5 Data analysis

4.5.1 Quantities from/treatment of SEM images

The SEM images were obtained as grayscale $512\text{ px} \times 512\text{ px}$ images.

```
//*** write if analysis of SEM images get analyzed ***
```

The images were then analyzed using ImageJ software.

4.5.2 Treatment of electrochemical data

The main quantities measured during the electrochemical cycling were time, current, and cell potential. This data was handled in Python. The time was shifted such that the data for each cell began on zero when the SEI formation started. For the Li deposition, the charge passed (per electrode area) was calculated. Charge passed (mAh cm^{-2}) is in this context defined as the deposition current (mA) divided by the Li area (cm^{-2}) integrated with respect to time (h) during the deposition step. Plotting the deposition as cell potential versus the charge passed, instead of versus time, makes comparison of the curves easier for different $J_{\text{deposition}}$.

5

Results and discussion

5.1 SEM images

Figure 5.1 shows SEM images of an unpolished and a polished piece of Cu with some deposited Li. To minimize the influence of a rough surface on the nucleation, it is clear that the samples should be polished. This also leads to more clean SEM images of deposited Li, where it is easier to separate the deposited Li from the surface features.

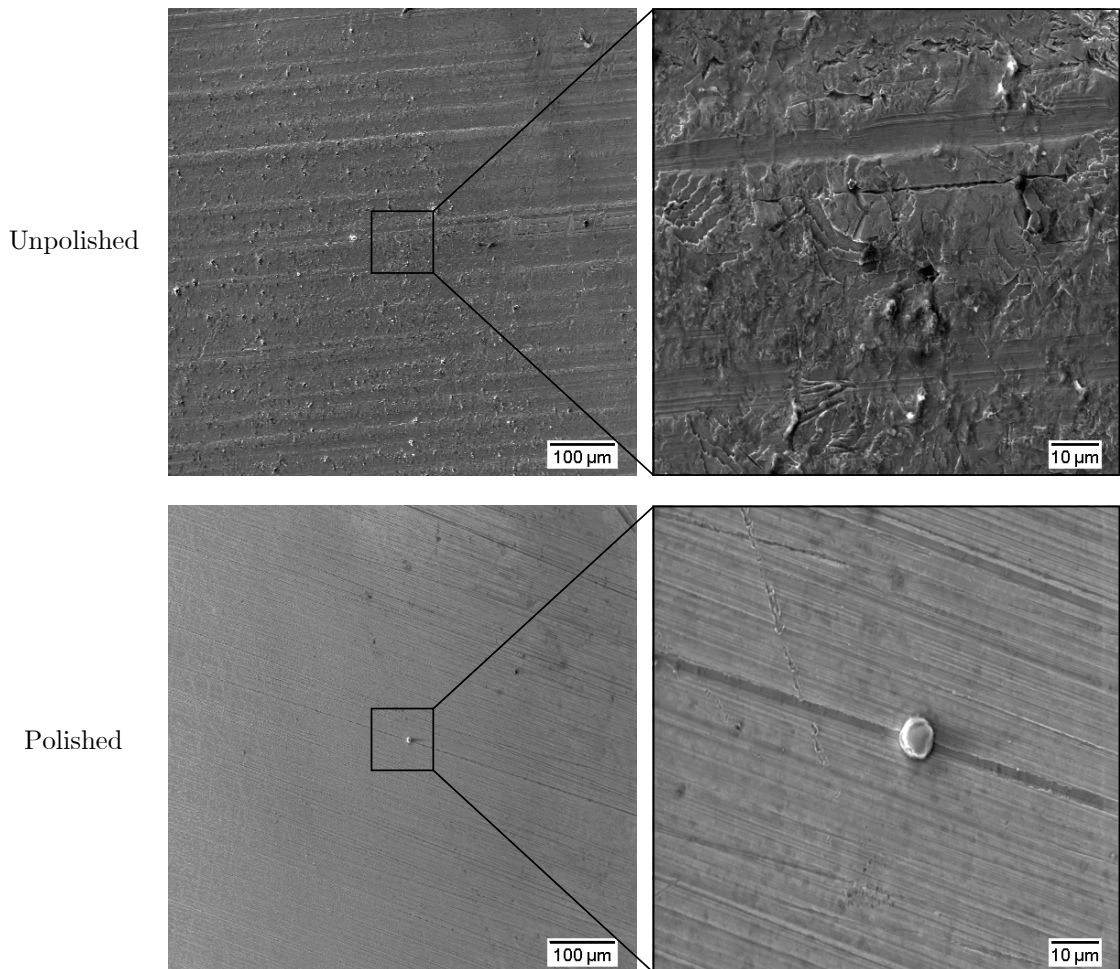


Figure 5.1. SEM images of an unpolished and polished Cu surface with some deposited Li. The polished Cu have substantially smaller surface roughness compared to the unpolished surface, resulting in easier identification of deposited Li and a cleaner image.

Figure 5.2 compares SEM-images of Cu surfaces in different cases of washing. The first row shows the result of no washing after having put only LiFSI electrolyte on the Cu surface. Large dark areas of electrolyte can be seen that obstruct the view. The second row shows that a bad rinse with DME after deposition of Li can leave behind large dark areas on the surface that seem to cover the deposited Li underneath. The dark areas reacted with the electron beam and started to bubble when imaged. Rinsing was perceived as an unreliable washing method and thus another method was tried. The third row shows the deposited Li after immersing and letting the Cu rest for 1 min in DME. However, some of the deposited Li might have had time to react in the DME bath, seemingly leaving behind smaller localized dark spots. Other washing times were tested, both 10 s and 5 min. The shortest duration of 10 s failed to remove all large dark areas, while the longer 5 min wash showed little improvement over the 1 min wash. Thus, washing of the surface was necessary and the immersion in DME for 1 min was deemed the best, showing sufficient removal of electrolyte while minimizing the potential reaction of deposited Li with the washing solvent.

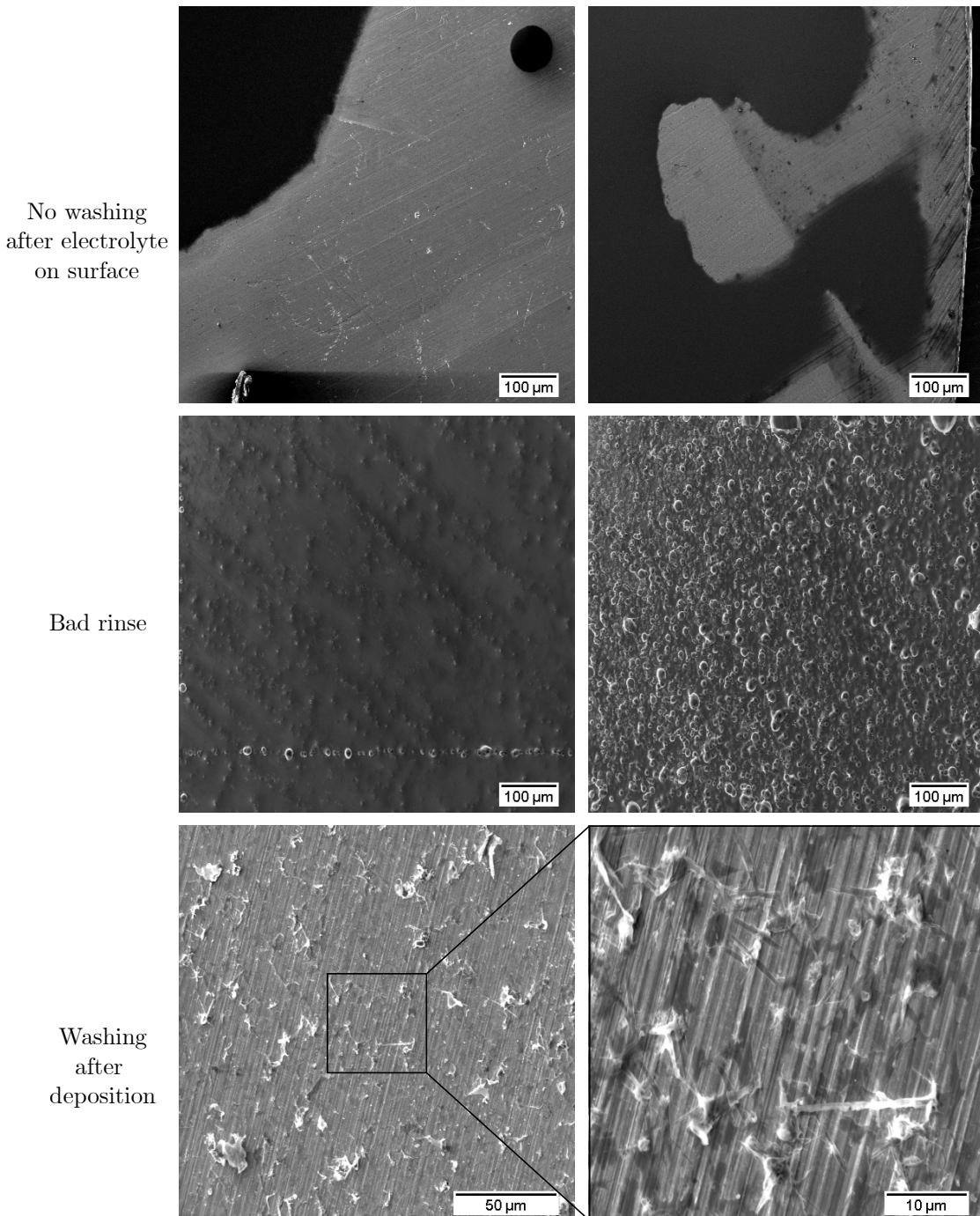


Figure 5.2. SEM images of Cu surfaces after various treatments. No washing leaves large dark parts of electrolyte that covers and obscure the surface beneath it (images at different places). A bad rinse of DME can leave enough electrolyte on the surface such that it bubbles when exposed to the electron beam (images taken at the same place at different times). Washing by immersion for 1 min in DME results in no large dark parts, however smaller dark spots can be seen, which could be deposited Li that have reacted.

5.1. SEM images

Figure 5.3 compares SEM images of deposited Li on Cu in a C-cell at different distances from the center of the deposition. The uneven deposition of Li on the Cu can be seen directly from the photograph. A gray annulus of deposited Li can be identified, meaning there is little to no Li at its center and significantly more along the outer edge of the annulus. Looking at the SEM images, it is clear that the morphology of the Li varies, from crystalline particles closer to the center and becoming larger, flatter 'islands' further away. Thus, the deposition of Li is uneven in a C-cell and the morphology depends on the radial position.

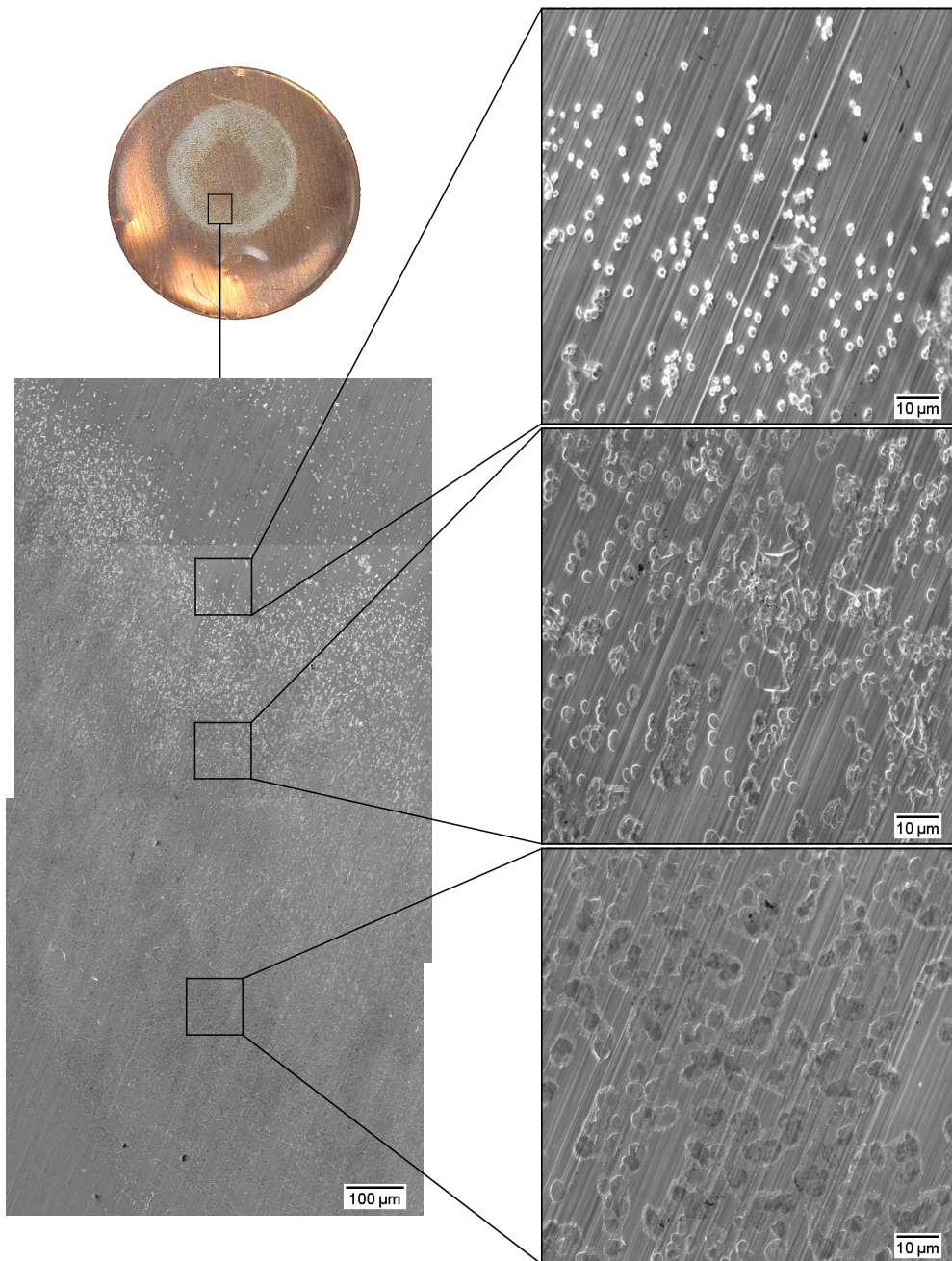


Figure 5.3. Different Li-morphologies along the radius for C-cells. The upper left photograph shows deposited Li (gray annulus) on Cu. The black rectangle on the Cu illustrates the position of the SEM images, which on the left-hand side have been overlaid (matching the features on one image with the features on the others). The SEM images on the right-hand side are magnifications of the ones on the left-hand side, showing different Li-morphologies, from small crystalline particles to larger and flatter 'islands', at different positions along the radius of the deposition.

Figure 5.4 compares SEM images of deposited Li on Cu in a C-cell at different positions along the edge of the deposition. The morphology here ranges from mostly 'bush'-like spaghetti to mostly particles. Thus, the morphology depends on the position along the edge of the deposition.

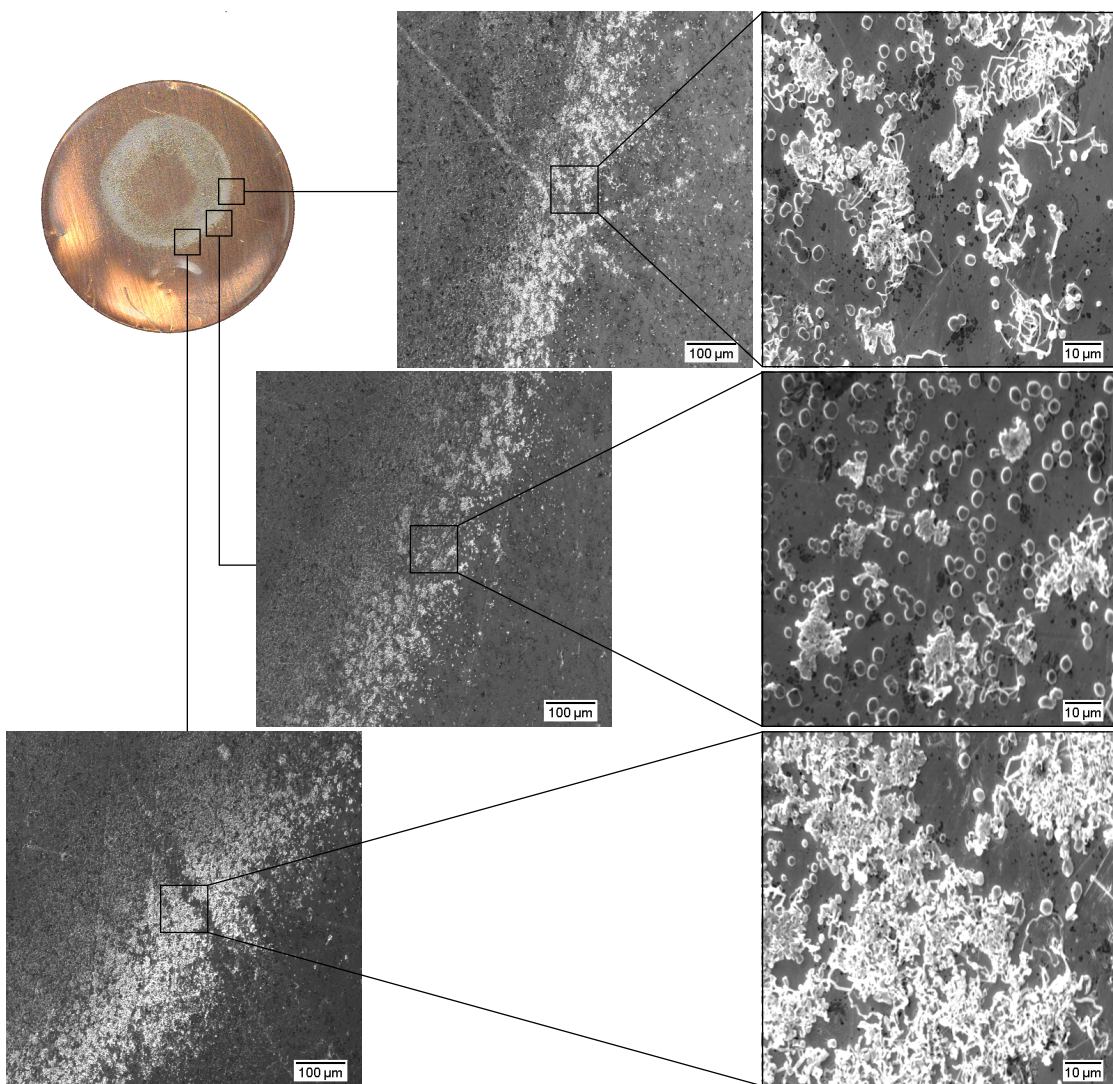


Figure 5.4. Different morphologies at the edge of the Li-deposition for C-cells. The upper left photograph shows deposited Li (gray annulus) on Cu. The black squares on the Cu illustrate the positions of the SEM-images. The SEM-images on the right-hand side are magnifications of the ones to the left. Different Li-morphologies, smaller particles or bush-like growth, are observed at different positions along the edge of the deposition.

Figure 5.5 shows SEM images of deposited Li on Cu in a T-cell at different positions.

//*** comment on more even Li on Cu surface if a photograph is taken later ***

The Li is much more evenly distributed compared to in a C-cell, with similar morphology observed throughout the deposited area. The morphology is mainly a mixture of particles and needle-like growth. This is unlike what was seen in the C-cell, but this can be due to the Li being more distributed instead of concentrated.

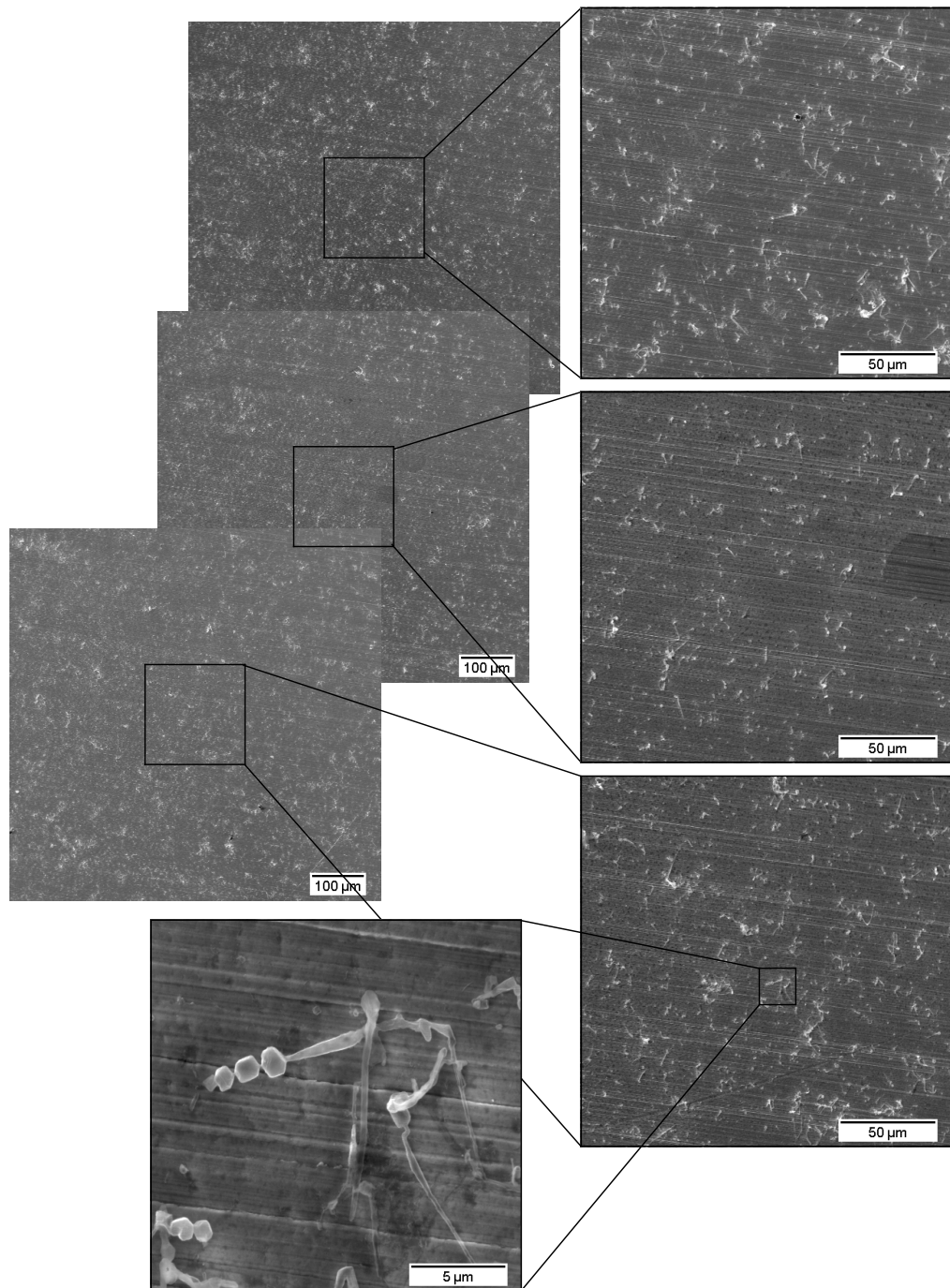


Figure 5.5. The deposition of Li in a T-cell is much more evenly distributed and with similar morphology over a larger distance compared to the C-cell (Figure 5.3 and Figure 5.4). The left-hand side shows overlaid SEM-images, and the magnified images to the right are representative over the entire area of the deposition. The highest magnification image shows that the Li-morphology is a combination of smaller crystalline particles about 1 μm in diameter, together with long and thin needle-like structures.

5.2 Electrochemical plots

For discussion of the electrochemical plots, the dimensionless variable σ and its meaning is introduced. Here, $\sigma = I_{\text{SEI-cutoff}}/I_{\text{deposition}}$, where $I_{\text{SEI-cutoff}}$ is the value (ignoring the sign) that when reached during the SEI formation, will stop the CV hold and start the CC deposition of Li at current $I_{\text{deposition}}$ (ignoring the sign). Thus, σ represents what fraction of the deposition current drives side reactions (including SEI formation) at the start of the deposition of Li.

5.2.1 Deposition for different degrees of substrate passivation

Figure 5.6 shows the current in a T-cell as function of time during the SEI formation by holding a constant cell potential of 0.010 V. During the SEI formation, reactions occur that passivates the electrode (Cu) surface, decreasing the current rapidly at first and then more slowly. The time taken to reach smaller values of σ in a T-cell increase rapidly, requiring only 1.7 min to reach $\sigma = 0.50$ and 2.0 h to reach $\sigma = 0.05$, but over 25 h to go below $\sigma = 0.01$ (all in the case of $J_{\text{deposition}} = 1 \text{ mA cm}^{-2}$). The choice of σ , at which point the SEI formation ends and the deposition starts, affects the subsequent deposition curve, see Figure 5.7.

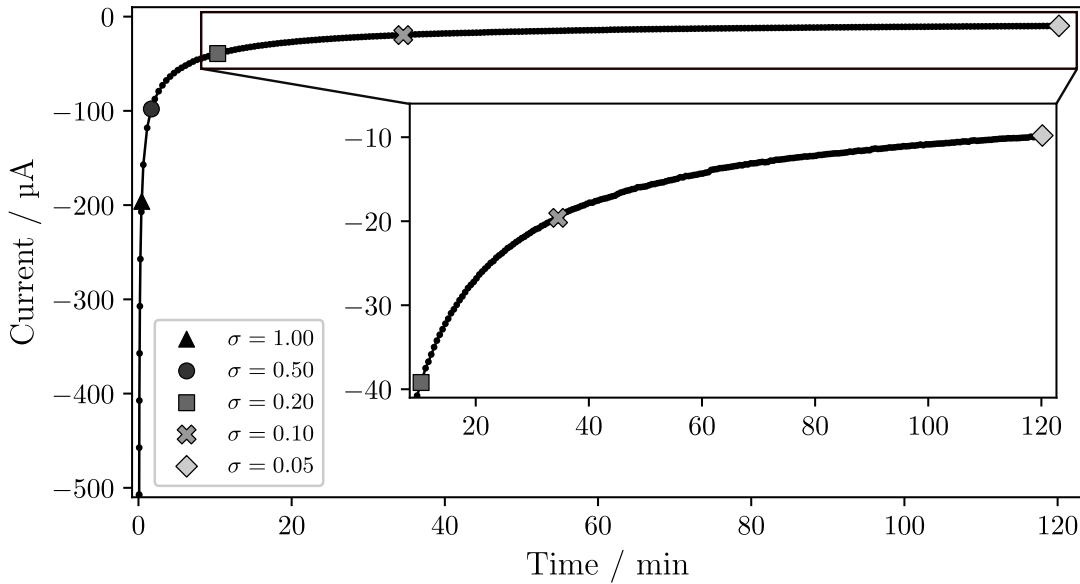


Figure 5.6. Current as function of time during the SEI formation by holding 0.010 V in a T-cell. Selected values along this curve are marked, where $\sigma = I_{\text{SEI-cutoff}}/I_{\text{deposition}}$ (in this case for $J_{\text{deposition}} = 1 \text{ mA cm}^{-2}$, or $I_{\text{deposition}} = -196 \mu\text{A}$).

The deposition curve, cell potential as function of deposited areal capacity, is

shown in Figure 5.7 for the different values of σ . For large σ , the current from side reactions are large enough to prevent obvious deposition. In other words, the side reactions are enough to drive the current without the necessity of Li deposition. For decreasing σ , a pronounced nucleation peak (the clear dip and then rise of the cell potential) becomes visible at around $\sigma \leq 0.20$. For sufficiently small currents of the side reactions, deposition of Li becomes necessary to supply the current and the nucleation peak presents itself. This trend is clearly demonstrated in Figure 5.7. Furthermore, it is evident that the choice of σ in measurements of deposition of Li affect the shape of the deposition curve. This should be taken into account when comparing and interpreting deposition curves.

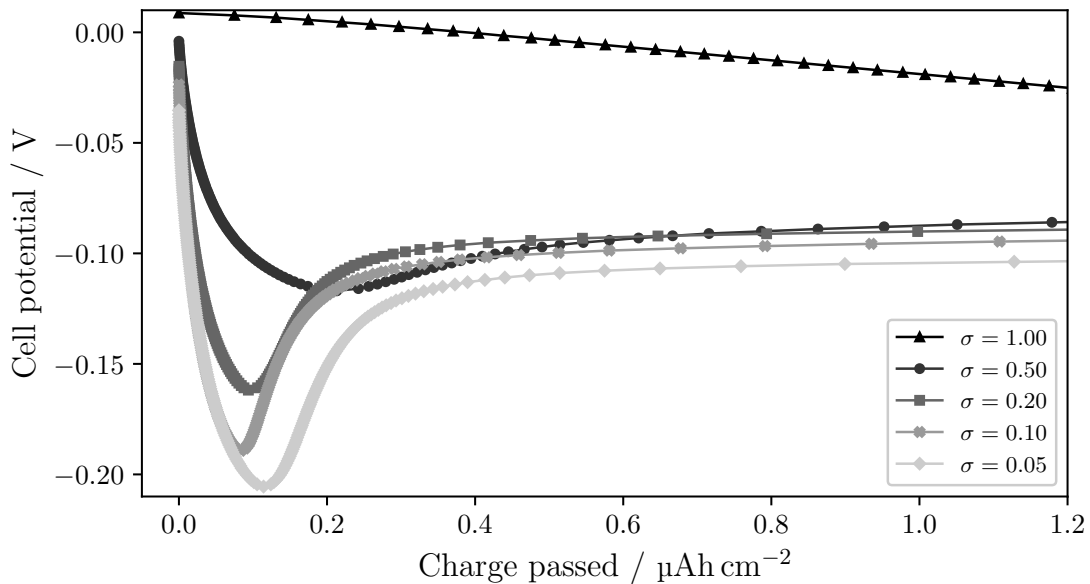


Figure 5.7. Cell potential as function of charge passed in T-cells, for different σ and $J_{\text{deposition}} = 1 \text{ mA cm}^{-2}$. For large σ (1.00 and 0.50), the applied current drives side reactions, and no nucleation peak is seen. For decreasing σ (0.20, 0.10, and 0.05), the nucleation peak becomes more and more pronounced, indicating that the absence of substantial side reactions enables more instantaneous nucleation.

5.2.2 Current density and cell configuration

Figure 5.8 compares the deposition curve for different $J = J_{\text{deposition}}$ for the T-cell, I-cell, and C-cell. For these measurements, $\sigma = 0.02$ except for the case $J = 0.10 \text{ mA cm}^{-2}$ in the T-cell, where $\sigma = 0.10$. Firstly, it is clear that higher J results in a lower cell potential for both nucleation and growth (higher overpotential). Secondly, the deposition peak gets smaller and disappears for increasing J in the I-cell and C-cell, but not in the T-cell. For $J > 5 \text{ mA cm}^{-2}$, the deposition curves for the I-cell and C-cell look more like the curve for $\sigma = 0.50$ in Figure 5.7. This implies that the $I_{\text{SEI-cutoff}}$ might have been high enough to affect the nucleation, despite using $\sigma = 0.02$. Figure 5.10 investigates this further.

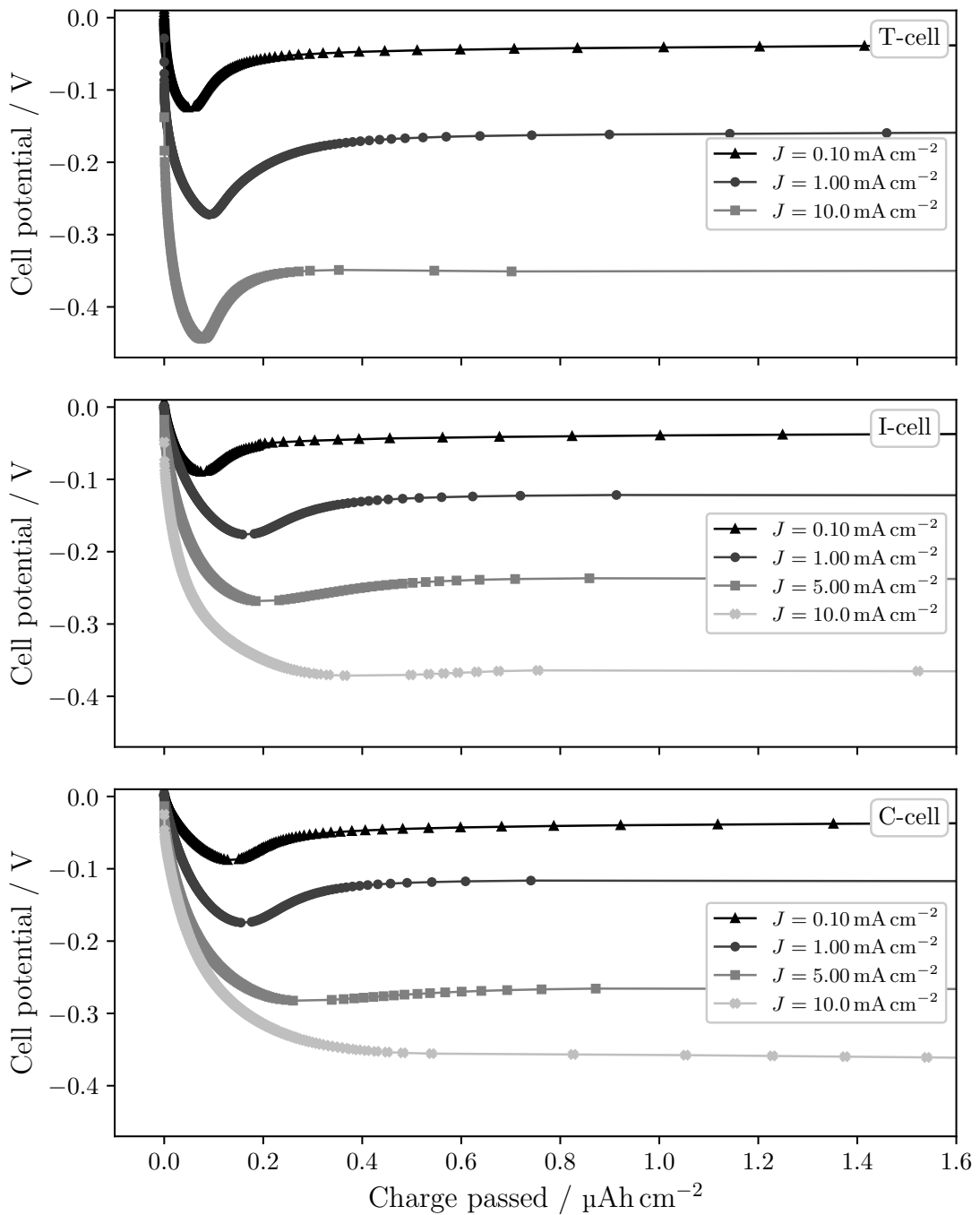


Figure 5.8. Comparison of deposition curves for different $J = J_{\text{deposition}}$ for a given cell configuration. For all measurements $\sigma = 0.02$ (except $J = 0.10 \text{ mA cm}^{-2}$ in the T-cell, where $\sigma = 0.10$). Larger J results in higher overpotential.

Figure 5.9 compares the deposition curve for different cell configurations for $J = J_{\text{deposition}}$ equal to 0.10 mA cm^{-2} , 1.00 mA cm^{-2} , and 10.0 mA cm^{-2} . For these measurements, $\sigma = 0.02$ except for the case $J = 0.10 \text{ mA cm}^{-2}$ in the T-cell, where $\sigma = 0.10$. The cell voltage is the lowest for the T-cell at the nucleation peak, but all cell configurations reach similar cell potential at the plateau region. This indicates that the cell configuration affects the nucleation more than the growth of Li.

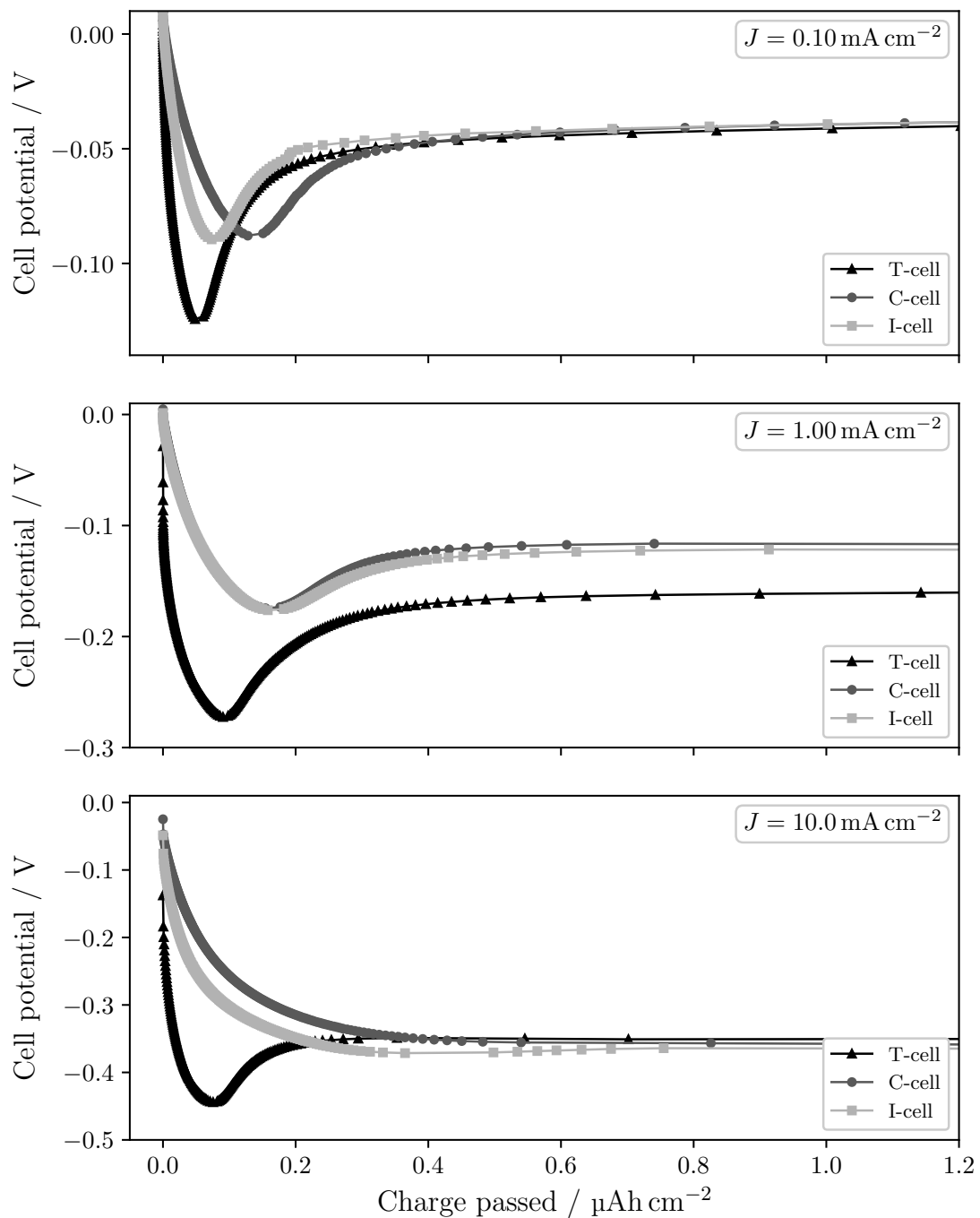


Figure 5.9. Comparison of deposition curves for different cell configurations for a given $J = J_{\text{deposition}}$. The nucleation peak is most prominent for the T-cell, while the curves look comparable for the C- and I-cell, though the curves seem slightly shifted to the right for the C-cell.

Figure 5.10 compares the deposition curve of $J = J_{\text{deposition}}$ equal to 1.00 mA cm^{-2} , 5.00 mA cm^{-2} , and 10.0 mA cm^{-2} for the C-cell for two cases. The first, where $\sigma = 0.02$, has already been shown in Figure 5.8 (and Figure 5.9), and the second is for a small and constant $I_{\text{SEI-cutoff}} = 0.392 \mu\text{A}$ (equal to $\sigma = 0.02$ for $J = 0.10 \text{ mA cm}^{-2}$). For each value of J , the lower value of $I_{\text{SEI-cutoff}}$ results in a deposition curve with a clear nucleation peak. Moreover, the cell potential reaches about the same value in the plateau region. The choice of $I_{\text{SEI-cutoff}}$ therefore seems to mostly affect only the nucleation process, and not the growth of the Li. Still, if all samples manage to grow the deposited Li, they must all have had nucleation. Thus, regardless of whether a clear nucleation peak is visible or not, nucleation must occur. Because the overpotential affects the rate of nucleation¹, whether progressive nucleation occurs (where some Li nucleate and start growing while others still nucleate) or instantaneous nucleation occur (where more or less all the nuclei nucleates at the same time, and then they all grow) might be the difference seen in Figure 5.10. In other words, whether the deposition curve ($J \geq 5 \text{ mA cm}^{-2}$) show a clear nucleation peak or not.

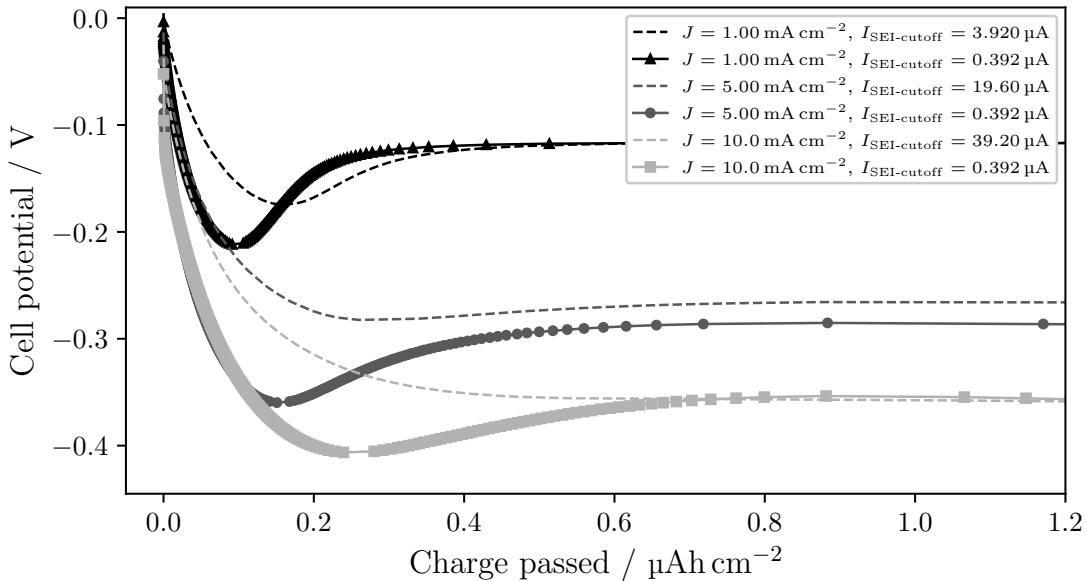


Figure 5.10. Comparison of the deposition curve for different $J = J_{\text{deposition}}$ and $I_{\text{SEI-cutoff}}$ for the C-cell. Comparison of the solid curves where $I_{\text{SEI-cutoff}} = -0.392 \mu\text{A}$, with the dashed curves where $\sigma = 0.02$, for each J . We see that the deposition peak is more pronounced for smaller $I_{\text{SEI-cutoff}}$, while more or less the same potential is reached in the plateau region.

¹Antar det eftersom overpotential påverkar nucleation energy barrier och reaction rate brukar vara exponentiellt beroende av energy barrier.

5.2.3 Different electrolytes

Figure 5.11 shows the current in the C-cell as function of time during the SEI formation by holding a constant cell potential of 0.010 V. Note the difference in timescale for the current in this case with the C-cell compared to that of the T-cell in Figure 5.11. Instead of taking 16 h to reach $\sigma = 0.02$ as in a T-cell, it only takes 20 min (for the same electrolyte, LiFSI). This could be due to the difference in pressure or in the volume of electrolyte, or both. The different electrolytes show the same trend in current over time, with the IL and LiFSI following each other closely. The passivation of the Cu took longer for the LiPF₆ up until a bit before the 10 min mark, where the current decreased faster and reached $I_{\text{SEI-cutoff}}$ about 5 minute before the two other electrolytes.

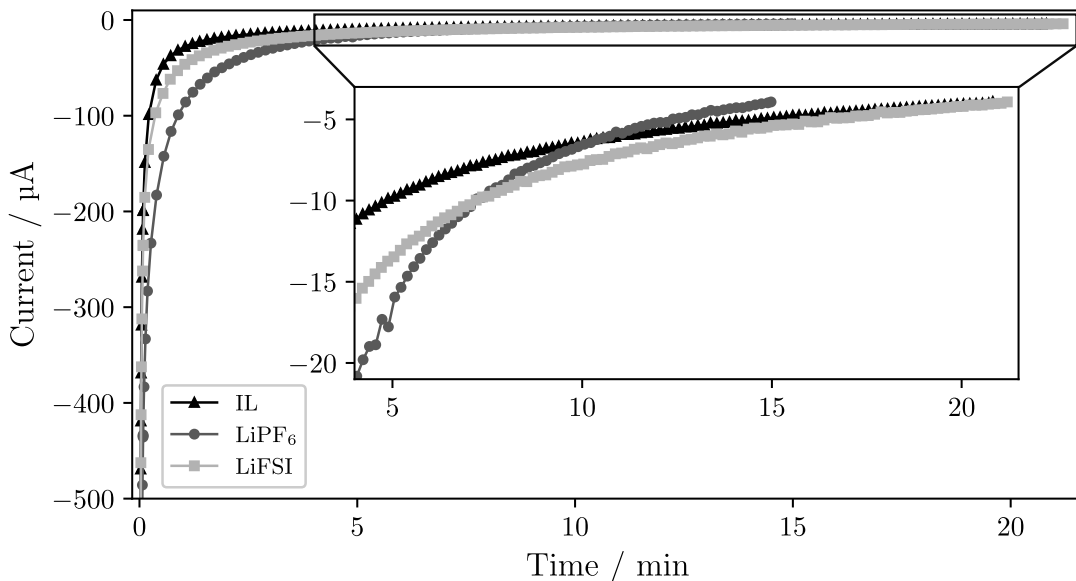


Figure 5.11. Current as function of time during the SEI formation by holding 0.010 V in C-cells with different electrolytes. In this case $\sigma = 0.02$, meaning $I_{\text{SEI-cutoff}} = 3.92 \mu\text{A}$ for $J_{\text{deposition}} = 1 \text{ mA cm}^{-2}$. In these cases, about 20 min was necessary to reach $\sigma = 0.02$, compared to the 120 min for $\sigma = 0.05$ in the T-cell (see Figure 5.6).

Figure 5.12 shows the deposition curves after the SEI formation in Figure 5.11 for different kinds of electrolytes in C-cells. The deposition curve is similar for the IL and LiFSI, while the LiPF₆ went lower in potential but had a less pronounced nucleation peak.

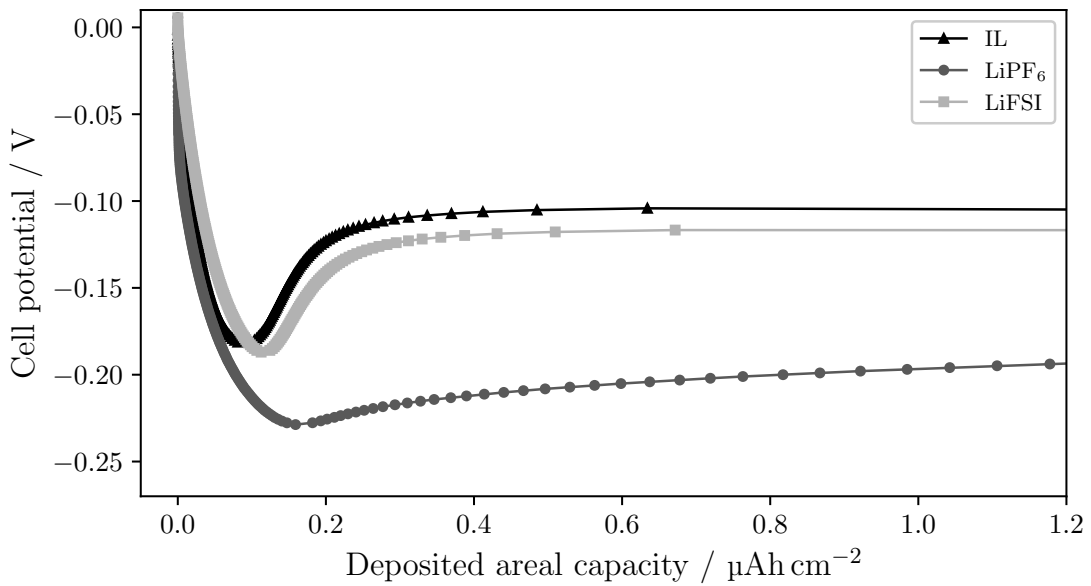


Figure 5.12. Comparison of the deposition curve for different electrolytes in the C-cell with $J_{\text{deposition}} = 1 \text{ mA cm}^{-2}$ and $\sigma = 0.02$.

6

Conclusions

// *** needs to be written cleanly after the results and discussion is finished ***

*** SEM ***

* Polishing and washing is necessary for clean SEM images. A 1 min wash of the Cu surface by immersion in DME was deemed the most suitable.

* C-cells result in Li-deposition concentrated in an annulus, probably due to uneven pressure from the wave spring(?) (or crimping of the cell?) (source?), and the morphology changes both radially and along the edge of the deposition. The morphology ranges from small crystalline particles, to larger and flatter 'islands', and even to bush-like growth, depending on the observed location on the Cu surface.

* T-cells result in deposition more evenly distributed over the Cu surface, where the observed morphology is rather smaller crystalline particles together with long and thin needle-like structures.

*

*** ELECTROCHEMICAL PLOTS ***

* The deposition curve depends strongly on the ratio $\sigma = I_{\text{SEI-cutoff}}/I_{\text{deposition}}$ of

the current at the end of the SEI formation, $I_{\text{SEI-cutoff}}$, and the current used for deposition, $I_{\text{deposition}}$ (ignoring the signs). The nucleation peak becomes more pronounced and deeper for decreasing σ , and for sufficiently large σ no nucleation peak is observed.

* The deposition curve also depends strongly on the current density used for deposition, $J = J_{\text{deposition}}$, where larger values of J means larger η_n and η_p .

* The T-cell showed a nucleation peak for high J ($=10$), even when the C-cell and I-cell did not.

* For high J , $\sigma = 0.02$ was found to result in a too high $I_{\text{SEI-cutoff}}$, where the nucleation peak did not appear. However, when choosing a lower $I_{\text{SEI-cutoff}}$, the nucleation peak appeared. Thus, the choice of $I_{\text{SEI-cutoff}}$ is highly influential on the shape of the nucleation peak and having a constant σ for different J might not be the most favorable method for comparing the nucleation peaks.

* Different electrolytes seemed to have some effect on the deposition, however this needs to be further researched.

References

- [1] B. Scrosati, K. M. Abraham, and W. van Schalkwijk, *Lithium Batteries: Advanced Technologies and Applications*. Wiley, 2013, ISBN: 9781118183656.
- [2] K. W. Beard, *Linden's Handbook of Batteries*, 5th ed. Mc Graw Hill, 2019, ISBN: 978-1-260-11592-5.
- [3] C. Xu, Q. Dai, L. Gaines, M. Hu, A. Tukker, and B. Steubing, “Future material demand for automotive lithium-based batteries,” *Communications Materials*, vol. 1, no. 99, 2020-10. DOI: <https://doi.org/10.1038/s43246-020-00095-x>.
- [4] B. V. Ratnakumar, M. C. Smart, R. C. Ewell, L. D. Whitcanack, K. B. Chin, and S. Surampudi, *Lithium-ion rechargeable batteries on mars rover*, version V1, 2004. DOI: 2014 / 38818. [Online]. Available: <https://hdl.handle.net/2014/38818>.
- [5] *Batteries for space power systems*, <https://ntrs.nasa.gov/citations/19690008710>, Report number: NASA-SP-172, Available online: <https://ntrs.nasa.gov/api/citations/19690008710/downloads/19690008710.pdf> (accessed: 2024-01-17), NASA, 1968-01.
- [6] *Cell*, Merriam-Webster.com Dictionary, (accessed: 2024-02-13). [Online]. Available: <https://www.merriam-webster.com/dictionary/cell>.
- [7] B. Scrosati and J. Garche, “Lithium batteries: Status, prospects and future,” *Journal of Power Sources*, vol. 195, no. 9, pp. 2419–2430, 2010, ISSN: 0378-7753. DOI: <https://doi.org/10.1016/j.jpowsour.2009.11.048>.
- [8] J. Deng, C. Bae, A. Denlinger, and T. Miller, “Electric vehicles batteries: Requirements and challenges,” *Joule*, vol. 4, no. 3, pp. 511–515, 2020, ISSN: 2542-4351. DOI: <https://doi.org/10.1016/j.joule.2020.01.013>.
- [9] D. Lin, Y. Liu, and Y. Cui, “Reviving the lithium metal anode for high-energy batteries,” *Nature Nanotechnology*, vol. 12, pp. 194–206, 2017-03. DOI: <https://doi.org/10.1038/nnano.2017.16>.

References

- [10] C. Fang, B. Lu, G. Pawar, M. Zhang, D. Cheng, and S. Chen, “Pressure-tailored lithium deposition and dissolution in lithium metal batteries,” *Nature Energy*, vol. 6, pp. 987–994, 2021-10. DOI: 10.1038/s41560-021-00917-3.
- [11] X. Shen, R. Zhang, P. Shi, X. Chen, and Q. Zhang, “How does external pressure shape li dendrites in li metal batteries?” *Advanced Energy Materials*, vol. 11, no. 10, 2021-01. DOI: 10.1002/aenm.202003416.
- [12] M. Sadd, S. Xiong, J. Bowen, F. Marone, and A. Matic, “Investigating microstructure evolution of lithium metal during plating and stripping via operando x-ray tomographic microscopy,” *Nature Communications*, vol. 14, no. 854, 2023-02. DOI: 10.1038/s41467-023-36568-z.
- [13] J. Qian, W. A. Henderson, W. Xu, *et al.*, “High rate and stable cycling of lithium metal anode,” *Nature Communications*, vol. 6, no. 6362, 2015-02. DOI: <https://doi.org/10.1038/ncomms7362>.
- [14] Z. Huang, G. Zhou, W. Lv, *et al.*, “Seeding lithium seeds towards uniform lithium deposition for stable lithium metal anodes,” *Nano Energy*, vol. 61, pp. 47–53, 2019-06. DOI: <https://doi.org/10.1016/j.nanoen.2019.04.036>.
- [15] X. Xieyu, J. Xingxing, K. O. O, *et al.*, “Diffusion limited current density: A watershed in electrodeposition of lithium metal anode,” *Advanced Energy Materials*, vol. 12, no. 19, p. 2200244, 2022-05. DOI: <https://doi.org/10.1002/aenm.202200244>.
- [16] A. Pei, G. Zheng, F. Shi, Y. Li, and Y. Cui, “Nanoscale nucleation and growth of electrodeposited lithium metal,” *Nano Letters*, vol. 17, no. 2, pp. 1132–1139, 2017-01. DOI: 10.1021/acs.nanolett.6b04755.
- [17] L. Qin, Y. Wu, M. Shen, *et al.*, “Straining copper foils to regulate the nucleation of lithium for stable lithium metal anode,” *Energy Storage Materials*, vol. 44, pp. 278–284, 2022, ISSN: 2405-8297. DOI: <https://doi.org/10.1016/j.ensm.2021.10.028>.
- [18] T. Balamurugan, H. T. Teka, H. Chen-Jui, *et al.*, “Nucleation and growth mechanism of lithium metal electroplating,” *Journal of the American Chemical Society*, vol. 141, no. 46, pp. 18 612–18 623, 2019. DOI: 10.1021/jacs.9b10195.
- [19] O. Crowther and A. C. West, “Effect of electrolyte composition on lithium dendrite growth,” *Journal of The Electrochemical Society*, vol. 155, no. A806, 2008. DOI: 10.1149/1.2969424.

- [20] A. Allerhand, “Who invented the earliest capacitor bank (“battery” of leyden jars)? it’s complicated,” *Proceedings of the IEEE*, vol. 106, no. 3, pp. 496–503, 2018. DOI: [10.1109/JPROC.2018.2795846](https://doi.org/10.1109/JPROC.2018.2795846).
- [21] M. V. Reddy, A. Mauger, C. M. Julien, A. Paolella, and K. Zaghib, “Brief history of early lithium-battery development,” *Materials*, vol. 13, no. 8, p. 1884, 2020-04. DOI: [10.3390/ma13081884](https://doi.org/10.3390/ma13081884).
- [22] M. Winter, B. Barnett, and K. Xu, “Before li ion batteries,” *Chemical reviews*, vol. 118, no. 23, pp. 11433–11456, 2018-11. DOI: [10.1021/acs.chemrev.8b00422](https://doi.org/10.1021/acs.chemrev.8b00422).
- [23] K. Schmidt-Rohr, “How batteries store and release energy: Explaining basic electrochemistry,” *Journla of Chemical Education*, vol. 95, no. 10, pp. 1801–1810, 2018-08. DOI: <https://doi.org/10.1021/acs.jchemed.8b00479>.
- [24] A. J. Bard, L. R. Faulkner, and H. S. White, *Electrochemical Methods: Fundamentals and Applications*, 3rd ed. Wiley, 2022-05, ISBN: 978 111 933 4064.
- [25] E. Andersson. “Spectroelectrochemical analysis of the li-ion battery solid electrolyte interphase using simulated raman spectra.” Uppsala Universitet, ISSN: 1401-5773. (2020-06), [Online]. Available: <https://www.diva-portal.org/smash/get/diva2:1442076/FULLTEXT01.pdf> (visited on 2024-03-25).
- [26] W. Zhang, E. Hosono, D. Asakura, *et al.*, “Chemical-state distributions in charged licoo₂ cathode particles visualized by soft x-ray spectromicroscopy,” *Scientific Reports*, vol. 13, no. 4639, 2023-03. DOI: [10.1038/s41598-023-30673-1](https://doi.org/10.1038/s41598-023-30673-1).
- [27] “Characteristics of lithium-ion batteries.” (2024), [Online]. Available: <http://www.electricity-magnetism.org/electric-battery/characteristics-of-lithium-ion-batteries/> (visited on 2024-03-25).
- [28] X.-B. Cheng, R. Zhang, C.-Z. Zhao, and Q. Zhang, “Toward safe lithium metal anode in rechargeable batteries: A review,” *Chemical Reviews*, vol. 117, no. 15, pp. 10403–10473, 2017-07. DOI: <https://doi.org/10.1021/acs.chemrev.7b00115>.
- [29] Y. Xu, K. Dong, Y. Jie, *et al.*, “Promoting mechanistic understanding of lithium deposition and solid-electrolyte interphase (sei) formation using advanced characterization and simulation methods: Recent progress, limitations, and future perspectives,” *Advanced Energy Materials*, vol. 12, no. 19, p. 2200398, 2022. DOI: <https://doi.org/10.1002/aenm.202200398>.
- [30] C. Soulen, N. Lam, J. Holoubek, and P. Liu, “Bridging the gap between pouch and coin cell electrochemical performance in lithium metal batteries,” *Journal of The Electrochemical Society*, vol. 171, no. 2, p. 020535, 2024-02. DOI: [10.1149/1945-7111/ad2731](https://doi.org/10.1149/1945-7111/ad2731).

References

- [31] V. Borovytsky, “Huygens–fresnel principle and abbe formula,” *Optical Engineering*, vol. 57, no. 9, 2019-09. DOI: <https://doi.org/10.1117/1.OE.57.9.095104>.
- [32] K. Vernon-Parry, “Scanning electron microscopy: An introduction,” *III-Vs Review*, vol. 13, no. 4, pp. 40–44, 2000, ISSN: 0961-1290. DOI: [https://doi.org/10.1016/S0961-1290\(00\)80006-X](https://doi.org/10.1016/S0961-1290(00)80006-X).

A |

Supplementary information: methods

Included below is further details of the methods and materials used.

A.1 Polishing of Cu

Below is further information about the polishing of Cu. Figure A.1 shows the grinding of the 70 mm × 70 mm Cu sheet. First, two edges of the Cu sheet were

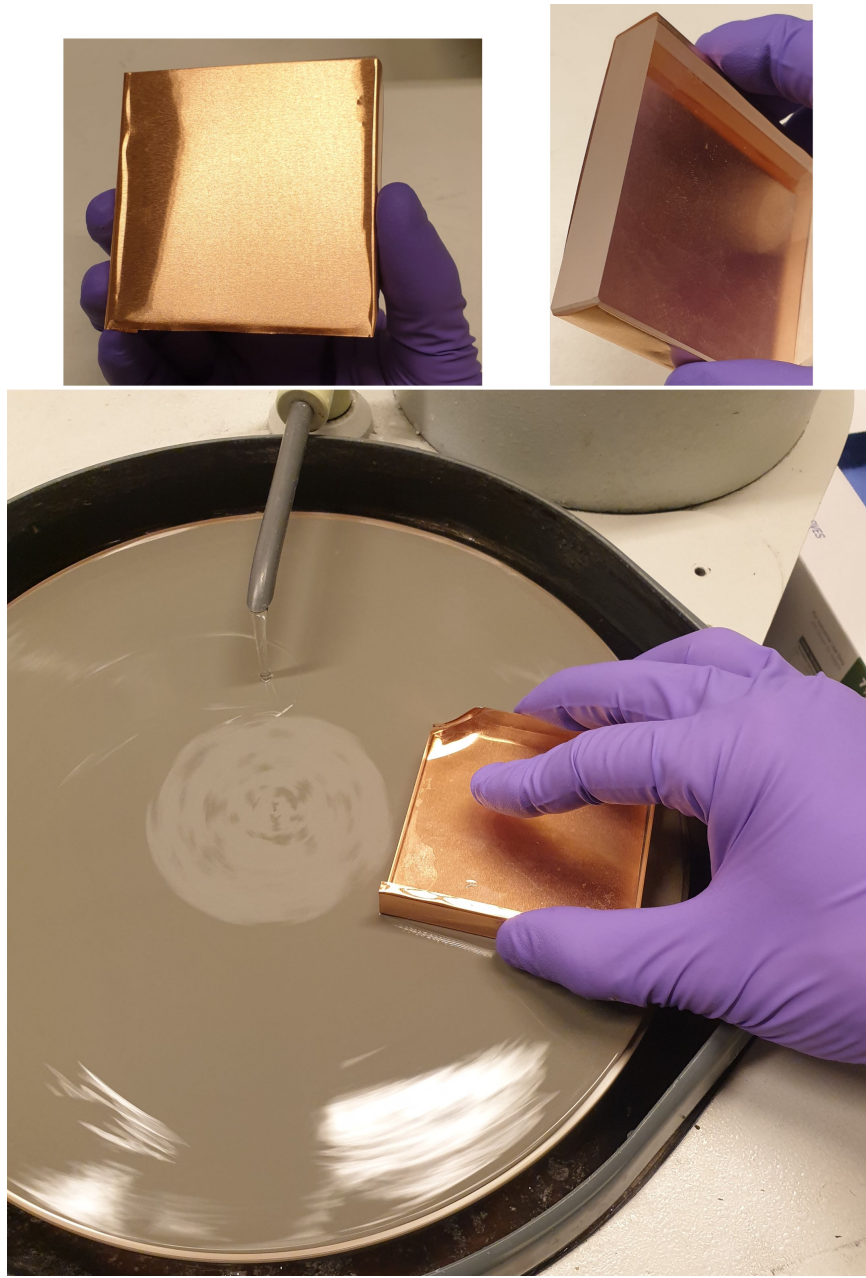


Figure A.1. Polishing of Cu using the grinder-polisher turntable from Buehler Beta.

bent around the edges of a flat piece of square glass. A grinding paper was then

placed center on the turntable and the water was turned on. During polishing, the grinding paper rotated while the Cu sheet was held in place by applying pressure on the edges of the glass using the fingers. An even surface polish was achieved by using the fingers to apply pressure on top of the glass in spots that at first received less grinding. Once an even surface polish was achieved for a given grinding paper, the next grinding paper was used. The following silicon carbinate grinding papers from Beuhler were used: P1200, P2500, and P4000, in order of polishing from coarser to finer. After the finest grinding paper, the Cu was blown dry using N₂ gas, put in a new plastic bag and sealed. Then followed the punching and cleaning as described in subsection 4.1.1.

A.2 Polypropylene spacer for T-cell

Figure A.2 shows the process of creating the 1 mm thick horseshoe-shaped spacers of PP. A cut was made with a scalpel from the edge of a 1 mm thick sheet of PP. A puncher 10 mm in diameter were used (along with a persuasive hammer) to punch out a circular piece where the cut was made. The piece was laid on the wooden board and another puncher, this time 7 mm in diameter, was centered and used to punch out the middle part. Due to the puncher being cone-shaped, the circular piece of PP expanded along the perimeter when the inner part was punched. Therefore, the cut done in the first step allows the PP piece to expand without becoming damaged during the last punching step. This worked significantly better than punching without a cut. Moving on, a few millimeters of the ring was cut away using a scalpel, creating an opening to inject the electrolyte when assembling the T-cell. Finally, a scalpel was used to clean up the edges.



Figure A.2. The process of punching the PP spacers. See text for explanation.

DEPARTMENT OF PHYSICS
CHALMERS UNIVERSITY OF TECHNOLOGY
Gothenburg, Sweden
www.chalmers.se



CHALMERS
UNIVERSITY OF TECHNOLOGY